Wireless passive weight sensor

Design and simulation of an RLC-resonance sensor for weight sensing in conveyor belts

Bachelor Graduation Thesis – TU Delft Electrical Engineering
19 June 2020

Rik Bokhorst (4700074) & Ruben van den Bos (4703375)

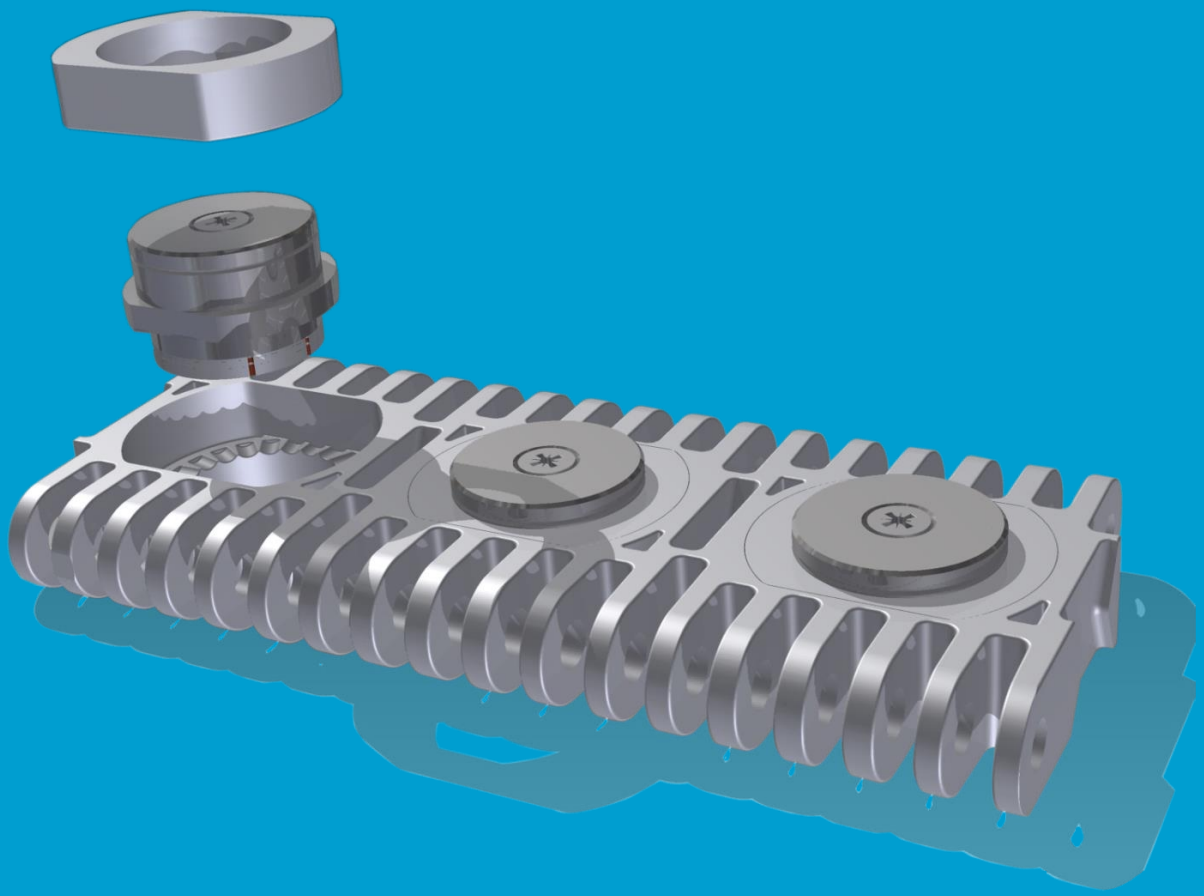

TU Delft Delft University of Technology

Challenge the future

Abstract

This thesis presents a resonant sensor circuit design that converts the deformation of a load cell in a conveyor belt into a change in resonance frequency. The sensor is inductively coupled to a reader circuit using planar PCB inductor coils. A sensor circuit was designed, fitted on a square PCB with 14.14 mm side length. The circuit consists of a planar squared inductor and a planar interdigital capacitor. The inductor has an inductance of 0.66535 μH, and the capacitor has a capacitance of 5.157 pF. An additional SMD capacitor was added to reach a resonating frequency range around 27.2 MHz. The deformation of the load cell causes a bend in the sensor PCB, which is directly attached to the diaphragm of the load cell. The bend causes a change in capacitance of the interdigital capacitor, which shifts the resonance frequency of the sensor. The sensor components are designed in MATLAB and simulated and verified in CST studio.

Preface

This bachelor thesis concerns the sensor design and simulation of passive wireless sensors for weight sensing on conveyor belts. It has been written to obtain a bachelor's degree in Electrical Engineering at Delft University of Technology. It is part of the Bachelor Graduation Project (EE3L11), which took place in the 4th quarter of the 3rd and final year of the bachelor. It was scheduled from the 20th of April 2020 until the 3rd of July 2020. The project was undertaken at the request of Intralox, a manufacturer of conveyance solutions and services designed to optimize product handling systems for manufacturers.

Unfortunately, the COVID-19 pandemic caused restrictions on on-campus activity. These restrictions meant students were not allowed to meet. Furthermore, the development of any physical prototype was forbidden in the context of this project. Therefore, no implementation of the design described in this thesis could be developed and tested. The paper is restricted to design, simulation, and discussion of the simulation outcomes. Nonetheless, the scientific level of the thesis was not affected, and probably even raised, since our focus was on exploring and gaining insight into concepts rather than practical skills.

We want to thank Intralox, and specifically Sven-Erik Haitjema and Lazlo Kleczewski, for this excellent opportunity to apply our knowledge and skills learned in our bachelor for commercial applications. Furthermore, we would like to thank Chris Verhoeven for exceptional guidance in these unusual times, and Ioan Lager for all effort in regulating this project and facilitating assistance. We would like to express our gratitude to Visweswaran Karunanithi for his support in understanding the simulation software. Lastly, we would like to thank our fellow students Jonathan Dijkstra, Rogier Fischer, Mauries van Heteren, and Jasper Insinger, for smooth communication and team work in times of online meetings. We are proud to look back at a successful project and engaging experience.

Rik Bokhorst & Ruben van den Bos
Delft, June 2020

Nomenclature

δ	Skin depth [m]
ω_{res}	Angular resonance frequency [rad/s]
ρ	Fill ratio of the coil
C_c	Capacitance of the interdigital capacitor [F]
C_l	Capacitance of the planar PCB coil [F]
C_s	Capacitance of the sensor [F]
C_{FR4}	Capacitance between the coil and the FR-4 material [F]
C_{SMD}	Capacitance of the SMD-capacitor that is placed in parallel with the sensor capacitor and coil [F]
d_{avg}	Average diameter of the coil [m]
d_{in}	Inner diameter of the coil [m]
d_{out}	Outer diameter of the coil [m]
g	Gap between two fingers of the interdigital capacitor [m]
h_c	Height of the copper strips of the interdigital capacitor on the FR-4 material [m]
h_l	Height of the copper strips of the coil on the FR-4 material [m]
k	Coupling coefficient of two coupled coils
K_1, K_2	Coefficients for the modified Wheeler formula, layout dependent [20]
L_1	Inductance of the readout coil [H]
L_2	Inductance of the sensor coil [H]
l_b	Length of the electrode base of the interdigital capacitor [m]
l_f	Length of a finger of the interdigital capacitor [m]
L_{mw}	Inductance calculated using the modified Wheeler formula [20] [H]
M	Mutual inductance between two coupled coils [H]
m	Margin between the interdigital capacitor model and the PCB edge [m]
n_c	Number of fingers of the interdigital capacitor
n_l	Number of turns of the coil
Q	Quality factor
R_1	Resistance of the readout coil [Ω]
R_2	Resistance of the sensor [Ω]
R_c	Resistance of the capacitor [Ω]
R_l	Resistance of the coil [Ω]
R_t	Turn-bend factor, typically 2.5
R_{st}	Sheet resistance of the coil [Ω/□]
s	Spacing between two turns of the coil [m]
w_b	Width of the electrode base of the interdigital capacitor [m]
w_f	Finger width of the interdigital capacitor [m]
w_l	Turn width of the coil [m]

Contents

1 Introduction

This chapter will introduce the project by defining the problem from which this thesis is originated. Subsequently, an overview is given of the surrounding total system. After that, a state-of-the-art analysis is given to provide background information on what already has been researched in the project's field and to mark the starting point of the design. In conclusion, a synopsis is given to outline the rest of the thesis.

1.1. Problem definition

Conveyor belts are able to transport packages with high pace, but the current system designed by Intralox makes use of an open feedback loop. Therefore, it is not able to detect whether products are in their desired positions. Besides, it is not possible to check whether there are errors in the products itself. The product may be weighed to solve these two problems. Nevertheless, with the current system, in order to weigh the products, transfers have to be carried out. The product has to leave the belt so that it may placed on a weighing scale, and afterwards, it may transferred to the next belt. This transfer causes many difficulties. The belts have to be synchronized, the transfers are not easy to carry out, and it slows down the conveying process [19].

Therefore, a conveyor belt consisting of small load cells of 2 cm in diameter was proposed. A product on the belt will exert weight on the load cells. The top-view and side-view of this conveyor belt are displayed in Figure 1.1. The directions shown in the overview are used from now on.

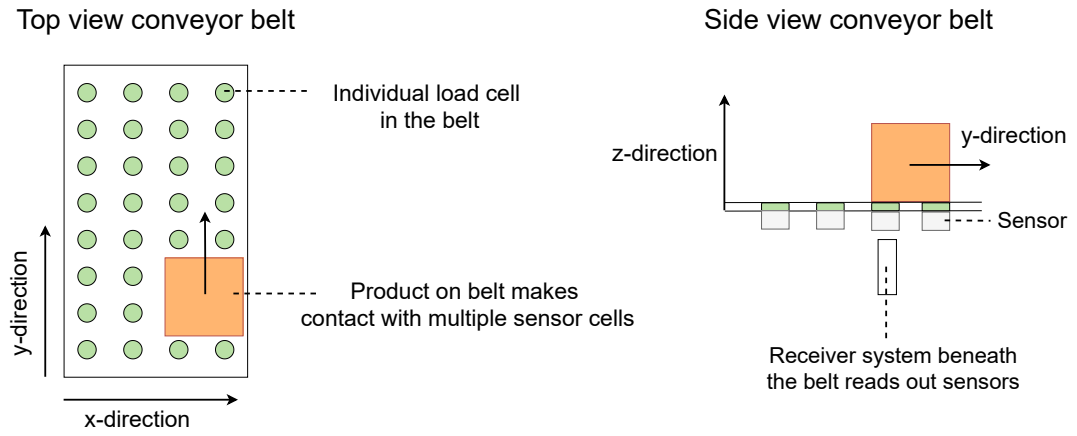

Figure 1.1: Top and side view of the belt with the load cells and sensors.

Intralox attempted to create a sensor in the belt to measure the weight and position of products while the belt is moving. A load cell was designed, which converts a mass into a bend of a diaphragm attached to the cell. See Figure 1.2 for an exploded view of this load cell. The screw may be used to alter the begin position of the diaphragm. Normally, the diaphragm is able to move from 0.0mm to 0.2mm. With the screw, this range may be shifted, for example from 0.1mm to 0.3mm.

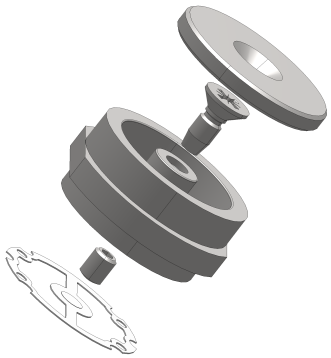

Figure 1.2: Exploded view of the load cell designed by Intralox.

The first sensor prototype consisted of a resonance circuit consisting of a capacitor and an inductor. The capacitor had two parallel plates which changed capacitance when they were brought closer together. The readout of the sensor was carried out using planar PCB coils. The resonance frequency was read out and converted into product weight. The position of the cell and readout coil impacted the results too much, causing inaccurate readouts. The second prototype consisted of capacitive dividers, also based on the parallel plate capacitor. A PCB with one antenna plate and multiple receiver plates were placed underneath the load cell to read out position, rotation and weight. The required sensitivity and uniformity of the receiver circuit made this design infeasible [19].

In order to improve the weighing system, a new sensor must be designed. This sensor has to be able to convert a mechanical deformation of the diaphragm of the load cell into a change in electrical parameters that is wirelessly read out and analyzed. For both the sensor and the wireless transfer component, physical dimensions and the type (i.e. capacitive or inductive) may be altered. Moreover, the electrical parameter that contains the signal may be chosen (i.e. voltage, current). The performance of the design is determined by evaluating the change of the chosen electrical parameter between the minimum and maximum deformation and by measuring the percentage of power transferred between the coils.

1.2. System overview

The sensor is measured by a readout circuit. The design of the reader is discussed by Fischer and Insinger [15]. The acquired data will be processed by an analyzer circuit, designed by Dijkstra and Van Heteren [9]. The three subsystems are displayed in Figure 1.3. Note that this figure is simplified; the actual circuits and block diagrams are discussed in more detail in the separate theses. Appendix D shows the design options for the three separate parts of the system.

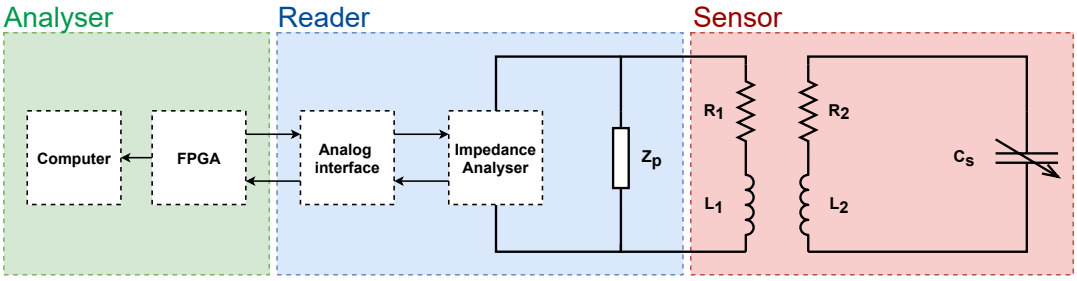

Figure 1.3: The circuit of the system.

1.3. State-of-the-art analysis

In order to design a passive sensor that converts pressure into a change in electrical parameters, several sensor types were investigated, namely capacitive sensors (parallel plate and interdigital capacitor), strain gauges, a coil sensor, piezoelectric sensors and antenna sensors. Many of these sensors are read out wirelessly. They are often used in medical applications [4] or for air pressure sensing [13][1][3]. Another common application is structural health monitoring [6][12][16][7], where the sensors sense strain in constructions to detect damage in an early stage. Pressure sensors are also applied in automotive [21] or aeronautical industries [17], using an LC-resonator or EM-transducer.

There are three ways to establish a wireless coupling between the sensor circuit and the readout circuit: inductive coupling, which is the most popular method [11], capacitive coupling, and electromagnetic coupling. For most sensors explained in this section, inductive coupling is used, utilizing coupled coils. For some sensors, especially antenna sensors, electromagnetic coupling is used. Capacitive coupling is rarely used, because of the small power density due to the small coupling capacitance [11].

A sensor that is much used is the capacitive sensor [1][13][18][21]. The capacitor often forms a resonance circuit together with an inductor. By deforming the capacitor, the capacitance changes, which shifts the resonance frequency of the sensor circuit. Different kinds of capacitors are used. Akar *et al.* [1] discuss an absolute wireless pressure sensor that consists of a capacitive sensor and a gold-electroplated planar coil. Hernández-Sebastián *et al.* [13] discuss a medical wireless touch mode capacitive pressure sensor (TMCPS) to measure ventricular blood pressure of the heart. Jia *et al.* [18] give a design of a passive wireless strain sensor using a planar interdigital capacitor with a series-connected inductor. The resonance frequency of the sensor changes when pressure is applied to the capacitor. Nabipoor *et al.* [21] use a capacitive sensor together with inductive coupling that measures both pressure and temperature.

Besides a capacitor, other components may be used as a sensor. Butler *et al.* [5] use an inductor as a sensor. In parallel to the inductor, a capacitor is placed to form a resonator. By impressing the inductor, the inductance changes, which changes the resonance frequency. Demori *et al.*[8] discuss resonating wireless sensors using an electro-mechanical piezo electrical resonator. Another type of pressure sensors is a strain gauge. It is not expensive, easy to install and sensitive to applied force [12]. By varying the resistance in the sensor circuit, the measured output of the sensor would either be a voltage or current. A strain gauge is not easy to read out wirelessly because the position of the sensor is not fixed.

A relatively new type of sensor is the antenna sensor. This sensor is based on the principle that a reader sends an electromagnetic signal to the sensor. This signal is scattered back to the reader by the sensor. The circuit works as a sensor and antenna at the same time. Dai *et al.* [6] discuss this type of sensor used in structural health monitoring.

A lot of research to wirelessly interrogated sensor circuits has already been carried out. However, none of the wireless sensors discussed in this section is used for weighing scale applications. A sensor has to be designed, possibly using one of the techniques explained in the articles, which delivers the desired characteristics. It needs the right dimensions, it must be read out at different distances, and it must be invariant to positional errors and temperature differences.

1.4. Thesis synopsis

This thesis starts with a program of requirements for the sensor in Chapter 2. These requirements will ensure that the sensor functions properly, that the ranges stay between certain bounds and that the sensor will work together with the other subsystems. Chapter 3 explains the design of the sensor. It discusses the design choices in detail and proposes dimensions and parameters for the components of the design. This design is then simulated. The results of the simulation are shown in Chapter 4. These results are then elaborately discussed in Chapter 5. Finally, a conclusion of the project is drawn in Chapter 6, in which also recommendations for future research will be given.

2

Programme of requirements

This chapter provides the requirements for the total system, the sensor subsystem and the interface between the sensor and the reader subsystem. The requirements for the total system are not only dependent on the sensor design, but also on the design of the reader and the analyser. The reader-sensor interface requirements are determined to ensure proper functioning between the sensor and the reader. Note that both mandatory requirements (MR) and trade-off requirements (ToR) are given. Mandatory requirements are most important; they are necessary to be met in order for the project to be successful. Intralox formulated most of the requirements in the project proposal [19]. The requirements without direct impact on the design of the sensor are found in Appendix C.

Project requirements

System requirements

Table 2.1: Requirements for the complete system

ID	Requirements for the design of the complete system.
SYS-MR01	The sensor shall be able to pass over information to the receiver moving with 2 m/s'.
SYS-MR02	The sensor shall be read out using a wireless method.
SYS-ToR01	The sensor should preferably be invariant for temperature differences in the range of 0 °C to 50 °C.

Sensor requirements

Table 2.2: Requirements for the design of the sensor.

ID	Requirements for the design of the sensor.
SEN-MR01	Deformation of the loadcell diapraghm (maximum 0.2 mm) shall result in changed electrical parameters of the sensor.
SEN-MR02	The sensor shall be invariant to positional errors of the coupling $\pm$3 mm in the x-direction.
SEN-MR03	The sensor shall be coupled to the reader for distances of 1-4 mm in the z-direction.

Table 2.2 – *Continued from previous page*

ID	Requirements for the design of the sensor.
SEN-MR04	The receiver shall be able to read the sensor with rotational errors of: • +/- 10 degrees in the width (X) dimension of the belt, due to mechanical placement and belt module tilt. • +/- 5 degrees in the length (Y) dimension of the belt, due to mechanical placement. • +/- 5 degrees in the height (Z) dimension due to mechanical placement
SEN-MR05	The sensor shall be passive, in the sense that it shall operate without the need to be connected to a power supply.
SEN-ToR01	The sensor should have a diameter of at most 2.0 cm.
SEN-ToR02	The sensor should preferably cost less than €1,-.
SEN-ToR03	The sensor should preferably have a resonance frequency between 26.965 MHz and 27.405 MHz.
SEN-ToR04	The sensor should preferably consist of one single piece of PCB material.

Reader-Sensor Interface Requirements

Table 2.3: Requirements for the interface between the reader and the sensor.

ID	Requirements for the interface between the reader and the sensor.
IF2-MR01	The sensor shall use coupled coils to transfer energy from and to the reader.
IF2-MR02	The sensor value shall be read by the reader independent of the coupling coefficient k.
IF2-ToR01	The resistor R_2 should not exceed 0.25Ω.
IF2-ToR02	The capacitor C_s should be larger than 1pF.
IF2-ToR03	The capacitor L_2 should be so that the quality factor is » 100.
IF2-ToR04	The capacitor C_l should not exceed $\frac{C_s}{10000}$.
IF2-ToR05	The sensor should have a changing resonance frequency of at least 0.4 MHz.

3
Design

3.1. Choice of sensor type

In Section 1.3, several sensor technologies were discussed. The advantages and disadvantages of these sensor classes need to be evaluated. The types included were capacitive sensors, strain gauges, coil sensors, piezoelectric sensors and antenna sensors.

Capacitive sensors are subdivided into parallel plate capacitors and interdigital capacitors. Parallel plate capacitors are characterized by their simple design, but they are more difficult to fabricate with precision. Intralox already attempted a design utilizing this technology, as mentioned in Section 1.1, and arrived at an infeasible design. Furthermore, it is difficult to achieve trade-off Requirement SEN-ToR04, which is to preferably use one layer of PCB. The metal diaphragm may be used as one of the plates of the capacitor, see the first configuration in Figure 3.1. However, the distance between the plates would greatly influence the capacitance. According to Intralox, the margins in the industry make this configuration difficult. For this reason, the bendable interdigital capacitor is a better candidate. It may be designed with planar copper strips on one PCB, which will make the fabrication relatively cheap and simple. However, it is challenging to find a mathematical description of this design.

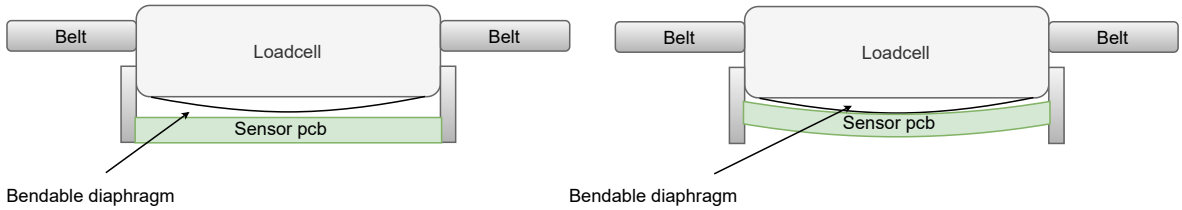

Figure 3.1: Two sensor configurations, with and without a bendable PCB.

Another class of sensor candidates is the strain gauge. Strain gauges are low-cost and widely used. However, strain gauges are used in combination with an amplifier to amplify the signal (as explained in Section 1.3). This amplification would make the sensor active, which does not meet Requirement SEN-MR05).

In addition, the coil sensor was examined. It is possible to apply pressure on a metal membrane that will bend towards the coil, or to apply pressure with the membrane on the sensor PCB directly, see Figure 3.1. The first option is very complex to realize because the distance between the load cell and the sensor would have to be precisely the same for every sensor. Small deviations in the fabrication process would influence the readouts. Furthermore, the metal membrane would also influence the readout coil. For the second option in Figure 3.1, the difference in inductance while bending would probably not be significant enough to cause a shift in the resonance frequency.

A piezoelectric resonator gives an electric output signal when a vibration is detected. When the product is on the belt, there will be no variation in pressure on the resonator so it will be challenging to acquire a usable output signal from the piezo sensor. Moreover, antenna sensors were considered. These sensors have simple design since only the antenna is needed and may be used both as a sensor and for wireless transfer. However, the antenna sensor was found to be too complex for the purpose of the

project.

After considering all the advantages and disadvantages of the sensors, the bendable planar interdigital capacitor is the most promising solution for the sensor.

3.2. Choice of wireless transfer component

For the wireless readout of the sensor, capacitive coupling, inductive coupling or EM-coupling are applicable. For capacitive coupling, as mentioned earlier in Section 1.3, there is a small power density available, which makes the coupling very difficult for the project's purpose. Furthermore, Intralox encountered too much complications when using capacitive coupling. EM-coupling would also not fit the project due to complexity of readout electronics involved at high frequencies. When using inductive coupling in combination with a capacitive sensor, the coil that is used for coupling may also be used to form a resonant circuit, which would simplify the design and make the sensor cheaper and easier to fabricate. Simplicity and low cost are essential because every cell in the conveyor belt will have a separate resonant circuit.

3.3. Circuit design

Figure 3.2 shows the circuit of the sensor. It consists of a resonant circuit with a variable capacitor (C_s) and an inductor (L_2). This resonant circuit is inductively coupled to the reader circuit, where inductor L_1 is the readout coil. Resistance R_1 is the resistance from coil L_1, and R_2 is the equivalent resistance of the sensor.

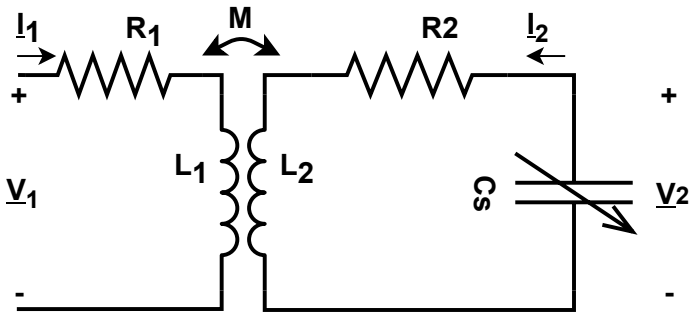

Figure 3.2: Capacitive sensor circuit

The mutual inductance $M = k\sqrt{L_1 L_2}$ may be used to reflect the impedance of the sensor circuit to the reader side, where the variable k is the coupling coefficient. The value of k ranges between 0 and 1, and expresses the coupling between the two coils. With $k = 1$, the two inductor coils are fully coupled, but with $k = 0$, there is no coupling. Voltage $\underline{V}_1$ and $\underline{V}_2$ is then expressed by Equation 3.1 and Equation 3.2, respectively.

$$\underline{V}_1 = R_1\underline{I}_1 + j\omega L_1\underline{I}_1 + j\omega M\underline{I}_2 \tag{3.1}$$

$$\underline{V}_2 = R_2\underline{I}_2 + j\omega L_2\underline{I}_2 + j\omega M\underline{I}_1 \tag{3.2}$$

Current $\underline{I}_2$ is equal to the current flowing through capacitor C_s, see Equation 3.3.

$$\underline{I}_2 = -\frac{\underline{V}_2}{1/(j\omega C_s)} = -j\omega C_s\underline{V}_2 \tag{3.3}$$

To get the equivalent impedance $\underline{Z}_{eq} = \underline{V}_1/\underline{I}_1$ at the reader side, Equations 3.1, 3.2 and 3.3 are used, see Equation 3.4.

$$\underline{Z}_{eq} = \frac{\underline{V}_1}{\underline{I}_1} = R_1 + j\omega L_1 + \frac{\omega^2 M^2}{R_2 + j\left(\omega L_2 - \frac{1}{j\omega C_s}\right)} \tag{3.4}$$

By using the substitutions in Equations 3.5 and 3.6 and rewriting the equations, Equation 3.7 is obtained, where ω_{res} is the resonance frequency and Q is the quality factor [22].

$$\omega_{res} = \frac{1}{\sqrt{L_2 C_s}} \tag{3.5}$$

$$Q = \frac{1}{R_2}\sqrt{\frac{L_2}{C_s}} \tag{3.6}$$

$$\underline{Z}_{eq}(\omega) = R_1 + j\omega L_1 \left(1 + \frac{k^2 \left(\frac{\omega}{\omega_{res}}\right)^2}{1 + j\frac{1}{Q}\frac{\omega}{\omega_{res}} - \left(\frac{\omega}{\omega_{res}}\right)^2} \right) \tag{3.7}$$

Requirement SEN-ToR03 specifies that the resonating frequency should lie between 26.965 MHz and 27.405 MHz. This band may be used without permission from the government in the Netherlands [10]. It was decided to make the resonance frequency range as large as possible, because it would be easier for the reader and the analyser team to achieve the desired resolution. By rewriting Equation 3.5 to Equation 3.8 and by making use of the frequency range, minimum and maximum bounds for the value of $L_2 C_s$ are found. The value of $L_2 C_s$ must lie between $3.373 \cdot 10^{-17} s^2$ and $3.4837 \cdot 10^{-17} s^2$.

$$L_2 C_s = \frac{1}{(\omega_{res})^2} \tag{3.8}$$

The values of L_2 and C_s are dependent on each other. Figure 3.3 shows different value combinations for $L_2 C_s$, see Appendix E.1 for the MATLAB script. The left figure shows the capacitance values for inductance values ranging from 0.5 μH to 3 μH. These inductance ranges are possible to be obtained for a planar PCB coil, but the accompanying capacitances, 10 pF to 60 pF, will be difficult to be obtained for an interdigital planar capacitor. An extra capacitor will be added in parallel to obtain the desired capacitance. The second figure shows how much the capacitance is allowed to change for the same range of inductance values in order for the frequency to remain between the bounds. These capacitance changes are maximum values, so when the capacitance changes more, the resonance frequency will go out of bounds, but when it changes less, it means that the resonance frequency range is shrinking.

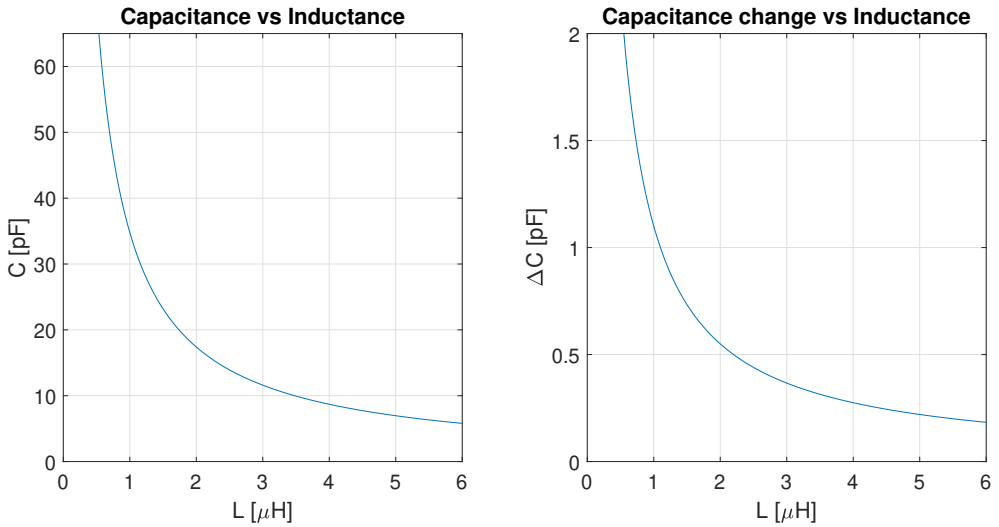

Figure 3.3: Capacitance and capacitance change versus inductance

3.4. Coil design

The main performance parameters of the planar inductor are the resistance and the inductance, which fully determine the quality factor of the inductor. By rewriting Equation 3.8 for C_2 and by substituting this in Equation 3.6, Equation 3.9 is obtained. This quality factor needs to be as high as possible in order for the impedance peak to be better detectable by the reader.

$$Q = \frac{\omega_{res} L_2}{R_2} \tag{3.9}$$

The equation shows that the quality factor increases with increasing inductance L_2 and decreases with increasing resistance R_2. The resistance may decreased by designing an inductor with fewer turns and wider traces, but on the other hand, the inductance increases with increasing n_l and decreasing w_l. For the resulting design trade-off, an optimal value is found for n_l and w_l for a maximum value of Q.

3.4.1. Modelling of a planar rectangular coil

To construct a planar rectangular coil, d_{in}, s, w_l, h_l, and n_l are specified as indicated in Figure 3.4. Starting from the middle at the distance given by d_{in}, every turn is built up. d_{out} is thus determined by the previously mentioned parameters. However, since the coil has a limited d_{out}, namely $\sqrt{2}$ times the specified maximum diameter of the sensor, d_{in} has been expressed as a function of d_{out}, s, w_l, and n_l according to the following equation:

$$d_{in} = d_{out} - 2(n_l + 1)w_l - 2n_l s \tag{3.10}$$

d_{out} is set to the maximum value, h_l to its minimum value of 0.07 mm, and s to its minimum of 0.09 mm. Increasing n_l will now increase d_{in} while keeping all other parameters constant. This is illustrated in Figure 3.5, where w_l is fixed.

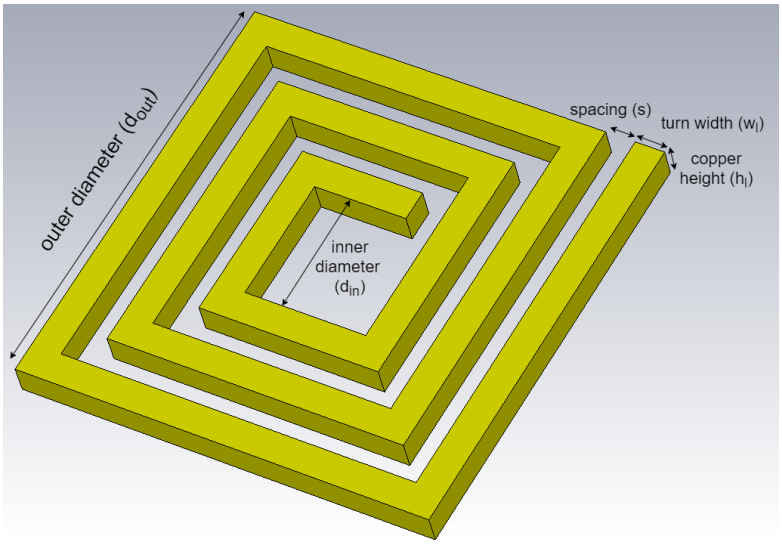

Figure 3.4: Model of planar rectangular coil with parameters

Subsequently, w_l is increased, resulting in an increase in d_{in}, while keeping n_l and all other parameters constant. It is concluded from Figure 3.5 that for every w_l, n_l may be increased until d_{in} as given by Equation 3.10 will become negative, which is physically impossible. This results in an equation that gives a maximum value of n_l ($n_{l,max}$), for every value of w_l:

$$n_{l,max} = \frac{d_{out} + s}{2(w_l + s)} \tag{3.11}$$

This maximum value is rounded down to an integer value. At $n_{l,max}$, the fill ratio ρ, given by Equation 3.12 will be equal to 1, since the coil is filled completely on the inside.

$$\rho = \frac{d_{out} - d_{in}}{d_{out} + d_{in}} \tag{3.12}$$

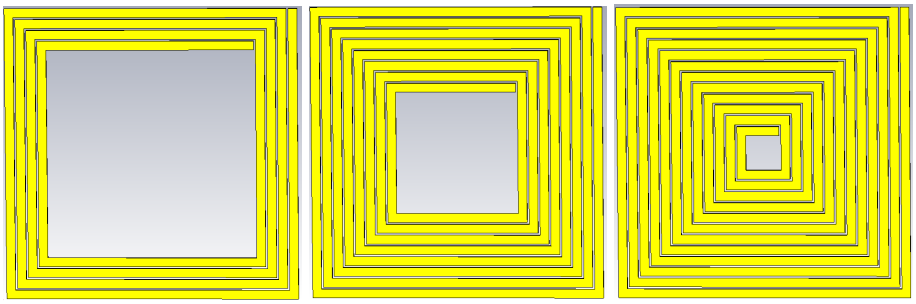

(a) n_l = 4 (b) n_l = 8 (c) n_l = 12

Figure 3.5: Coil model for varying n_l and d_{in} using Equation 3.17 and Equation 3.10, and with w_l = 0.4 mm

3.4.2. Planar inductor equivalent circuit

A planar PCB coil may be modelled by an equivalent circuit, see Figure 3.6 [2]. The capacitance C_p is caused by the capacitance between adjacent turns. L_{mw} is the inductance of the coil and R_l is the resistance. Finally, capacitance C_{FR4} is caused by the capacitance between the coil and the FR-4 material. The capacitances and resistance are parasitic components and need to be minimized for a good performance of the coil.

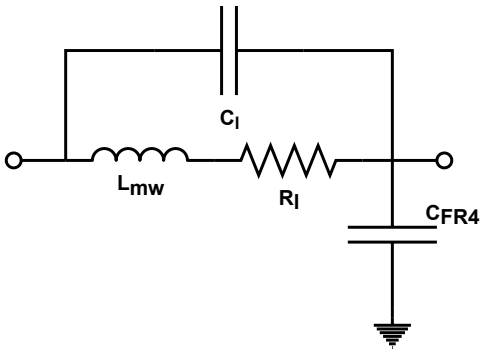

Figure 3.6: Lumped model of the planar PCB coil.

3.4.3. Inductance calculations

The inductance of a planar spiral coil may be calculated in three ways: using the modified Wheeler formula, the current sheet approximation or by data fitting [20]. The modified Wheeler formula is simple and around equally accurate as the other two methods. Therefore, the modified Wheeler formula (Equation 3.13) was implemented.

$$L_{mw} = K_1 \mu_0 \frac{n_l^2 d_{avg}}{1 + K_2 \rho} \tag{3.13}$$

For a square coil, K_1=2.34 and K_2=2.75. The formula was implemented in MATLAB. The MATLAB code (Appendix E.2) calculates the inductance for different numbers of turns. It stops when the maximum number of turns, according to Equation 3.11, is reached. It performs this calculation for various turn widths in the range of 0.10 mm to 0.50 mm. Figure 3.7 shows a plot of the inductance, where the black line indicates for which number of turns the inductance reaches its maximum at specific turn widths.

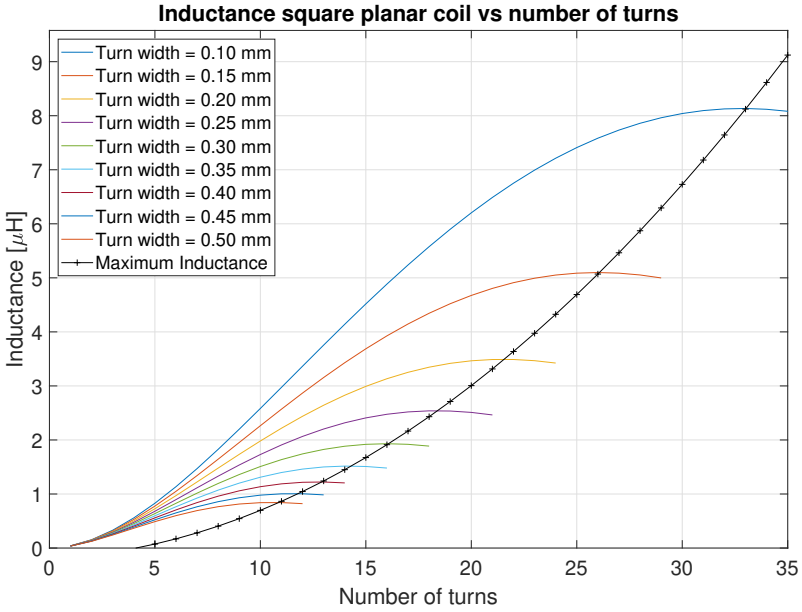

Figure 3.7: Inductance versus number of turns, s = 0.09 mm, h_l = 0.07 mm, d_{out}=14.14 mm

.

3.4.4. Coil resistance calculations

The total series resistance of a square spiral inductor may be calculated by adding resistance due to the skin effect, the sheet resistance, the proximity effect and the turn-bent resistance [18]. The skin depth is given by:

$$\delta = \sqrt{\frac{2\rho}{\omega\mu_0}} \tag{3.14}$$

At a frequency of 27 MHz, the skin depth will equal approximately 12.5 μm. This value is significantly lower than h_l (70μm). Therefore, the resistance due to the skin effect is neglected. Furthermore, the proximity effect is neglected for frequencies below 1 GHz. The sheet resistance is given by Equation 3.15, and is measured in Ω^2. For the bent factor R_t = 2.5 is taken [18]. The total resistance of the coil is given by Equation 3.16.

$$R_{st} = \frac{\rho}{h_l} \tag{3.15}$$

$$R_l = R_{st}\left[\frac{(4n_l - 2)(d_{in} + n_l s)}{w_l} + (2n_l - 1)(2n_l - 4) + 4n_l R_t\right] \tag{3.16}$$

Equation 3.16 calculates the resistance for a different number of turns and stops when the maximum number of turns is reached. Once more, turn widths are in the range of 0.10 mm to 0.50 mm. The plot of the resistance is depicted in Figure 3.8. This resistance should be minimized, which may be done by decreasing n_l and w_l. However, this will also affect the inductance, as was shown in Section 3.4.3. Therefore, it is better to look at the quality factor of the coil. The Q-factor is a function of both L and R_l.

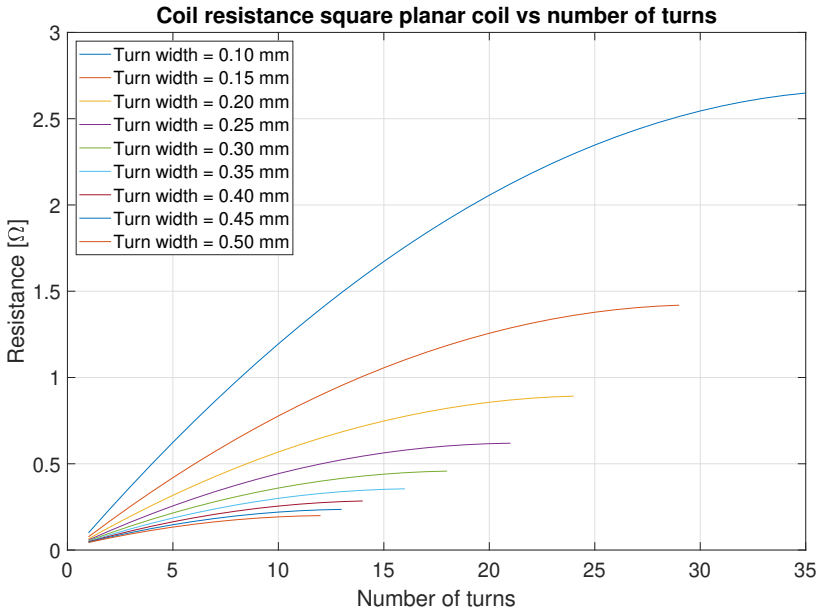

Figure 3.8: Resistance versus number of turns for different turn widths, s = 0.09 mm, h_l = 0.07 mm, d_{out}=14.14 mm

.

3.4.5. Coil quality factor calculations

The resistance and inductance determine the quality factor explained by Equation 3.9. The quality factor is plotted in Figure 3.9, where the maxima are again fitted by the black line. The quality factor needs to be as high as possible, which happens at w = 0.40 mm.

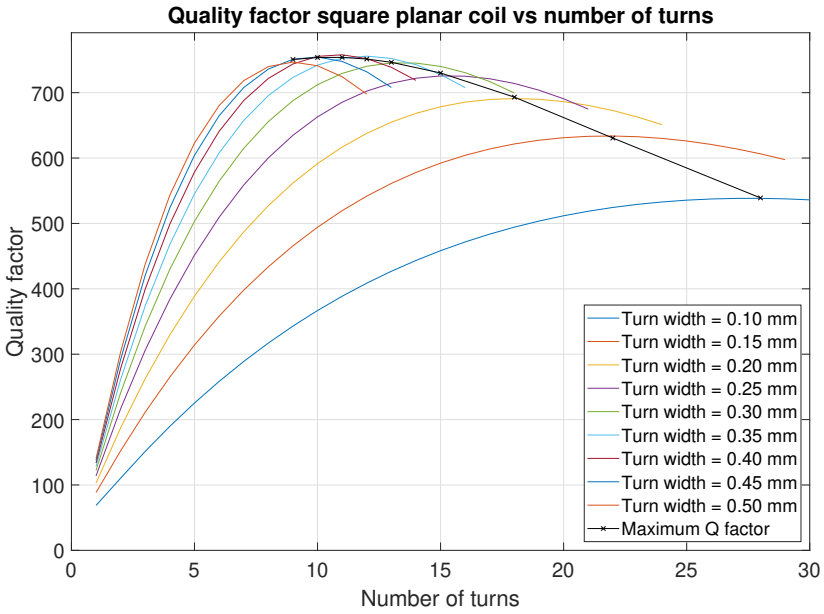

Figure 3.9: Quality factor versus number of turns, s = 0.09 mm, h_l = 0.07 mm, d_{out}=14.14 mm

.

3.4.6. Coil parameters

Table 3.1 shows the selected coil parameters and the theoretical calculated values.

Table 3.1: The parameters of the coil and calculated inductance, resistance and Q-factor.

Parameter	Value	Parameter	Value
n_l	11	s	0.09 mm
w_l	0.40 mm	ρ	0.60
h_l	0.07 mm	L (theoretical)	1.188 μH
d_{out}	14.14 mm	R (theoretical)	0.2659 Ω
d_{in}	3.54 mm	Q (theoretical)	757.9

3.5. Capacitive sensor design

3.5.1. Modelling of the interdigital capacitor

The square planar interdigital capacitor consist of two electrodes that both consist of a base with half of the specified number of fingers (n_c, always an even number) connected to it. In the adopted model, which is depicted in Figure 3.10, the two bases are at maximum distance from each other. Since the load cell on which the sensor is located has a circular shape with a diameter of 20 mm, l_b is limited to maximally $\sqrt{2}$ times this 20 mm, and the two bases are maximally spaced with $l_b - 2w_b$. On both sides a small margin m of 0.1 mm is taken.

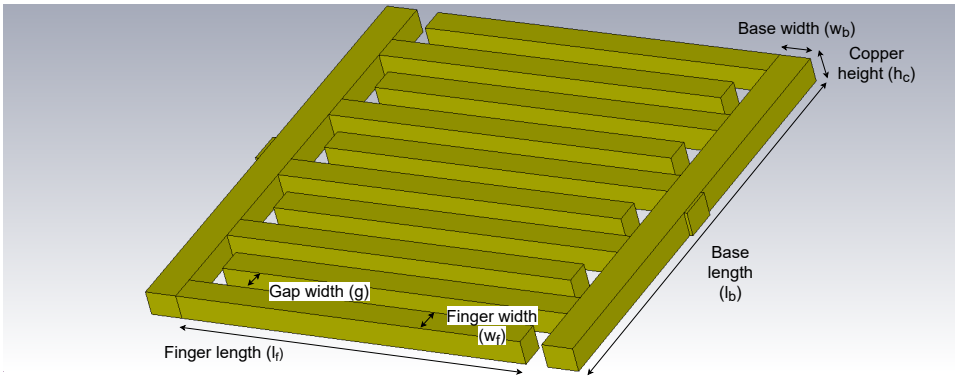

Figure 3.10: Model of interdigital capacitor with parameters

In order to determine a relationship between n_c and the capacitance, l_f and w_f were made dependent on l_b, w_b, g, n_c, and m, given by the following equations:

$$l_f = l_b - 2w_b - 2m - g \tag{3.17}$$

$$w_f = \frac{l_b - 2m + g}{n_c} - g \tag{3.18}$$

g is taken to be constant, namely 0.09 mm, which is the narrowest width that is possible for the PCB supplier of Intralox. g is the same between every finger and between the end of a finger and the base of the other electrode. h_c is minimized to 0.07 mm (2oz). w_b is set to 1.0 mm. Figure 3.11 shows three models with different number of fingers. The material is chosen to be annealed copper and the copper is placed on top of a FR-4 material board with thickness 0.2 mm. Intralox showed with measurements that using a thicker PCB, the mechanical deformation of the PCB would be permanent.

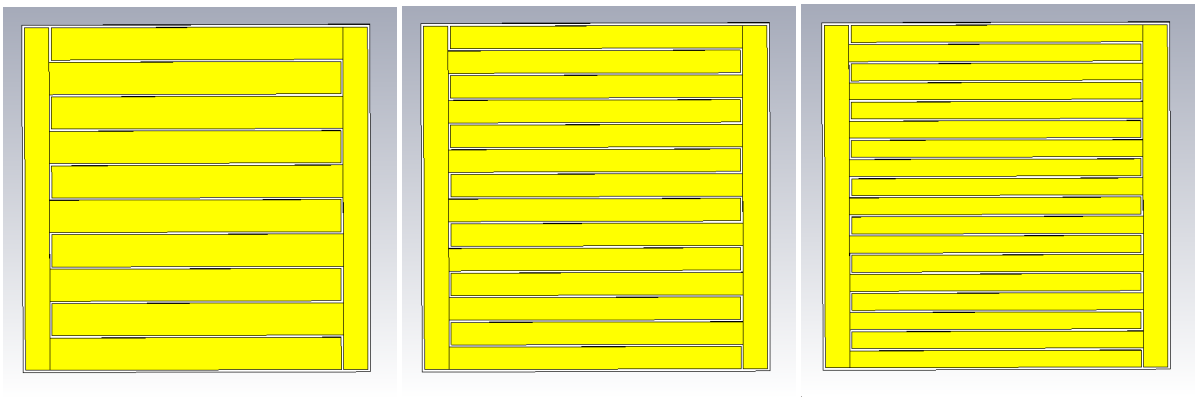

(a) n_c = 10 (b) n_c = 14 (c) n_c = 18

Figure 3.11: Inter-digital capacitor model for varying n_c and dimensions of fingers using Equation 3.17 and Equation 3.18.

3.5.2. Capacitor resistance

The interdigital capacitor also contains a resistance introduced by the skin effect [18]. This resistance is calculated using Equation 3.19 . With l_c =11.85 mm, f = 27 MHz, n_c = 10, w_f = 1.079 mm and g = 0.09 mm, the resistance becomes R_c = 0.0583 Ω. This resistance is in series with the coil resistance and thus influences the quality factor. With increasing number of fingers, the resistance gets smaller. This is why the capacitor must have as many fingers as possible.

$$R_c = \frac{4l_c\sqrt{\rho\pi\mu_0 f}}{3[n_c w_f + (n_c - 1)g]} \tag{3.19}$$

3.5.3. Capacitance calculation

The capacitance of an interdigital capacitor may be calculated by transforming the capacitor into a parallel plate capacitor using conformal mapping [18]. The capacitor consists of an infinite layer of air on top of the capacitor, and a finite layer, the substrate. In order for this method to work, the substrate must be thicker than λ/2, where λ is equal to the spatial wavelength of the capacitor: $\lambda = 2(w_f + g)$ [14]. This equation does not hold for this design. The equations for the conformal mapping may be adapted for a thinner substrate. However, that goes beyond the scope of this project. Therefore, it was decided to use the Finite Element Method (FEM). Using Electromagnetic simulations in CST Studio Suite®, the domain with the interdigital capacitor in it is divided into very small sub-domains, which is called a mesh. CST calculates the electric field using Maxwell's equations. Scattering parameters are calculated, from which the impedance and capacitance are calculated [24].

Using the method explained in Section 3.3 with the theoretical inductance of L=1.188 μH, the required capacitance is now calculated. This yields a capacitance of $C = 1/(L\omega^2)$=29.2 pF. Figure 3.3 shows that the maximum capacitance change is ΔC_{max} =0.9258·10^{-13} F, which is almost 1 pF. A capacitor with 72 fingers is chosen, which is the maximum number of fingers. This maximum will ensure the highest capacitance. Table 3.2 shows the dimensions and parameters of the capacitor. Also, the simulated capacitance and calculated resistance are shown. The capacitance is far below the value that is needed.

Table 3.2: The parameters of the interdigital capacitor, the simulated capacitance and calculated resistance.

Parameter	Value	Parameter	Value
n_c	72	g	0.09 mm
l_f	11.85 mm	h_c	0.07 mm
l_b	13.39 mm	C_c	5.157 pF
w_f	0.105 mm	R_c	0.0485 Ω

The required capacitance is $C_c = 29.2$ pF. Therefore, a physical capacitor (SMD) capacitor of 24.043 pF has to be placed in parallel to the interdigital capacitor to obtain the desired capacitance. An additional advantage of this is that the total resistance of the capacitor configuration decreases.

3.6. Coupled coil design

The design of the coil that forms the resonant circuit was given in Section 3.4. In order to wirelessly readout this resonant circuit, a second coil, the readout coil is designed. This coil is also part of the readout circuit of the overall system. As the sensor moves across the readout circuit, the coils need to be coupled as long as possible. In that case, the reader has enough time to obtain a useful signal. A longer coupling time is achieved with a larger readout coil. Nevertheless, the readout coil may not be larger than the sensor coil, because other sensors are placed next to this sensor in the belt. When the readout coil becomes more substantial than the sensor, it will also be coupled with other sensors, which will cause errors in the readout. Therefore, it was decided to use the same design for the sensor and readout coil.

The coupling factor and the inductances determine the mutual inductance of the two coils. This relationship is given by $M = k\sqrt{L_1 L_2}$. Since the coils are the same, this equation simplifies to $M = kL_2$. The mutual inductance was extracted from simulations with CST. Equation 3.20 is used to calculate the mutual inductance [23]. The $Z_{2,1}$ parameter is extracted from the scattering parameters obtained with the simulation. From the mutual inductance, the coupling factor is calculated with $k = M/L_2$.

$$M = \frac{Im\{Z_{2,1}\}}{\omega} \tag{3.20}$$

3.7. PCB design

The components designed in this chapter are implemented on a PCB, see Appendix A. The interdigital capacitor, inductor and SMD-capacitor were placed on a circular PCB so that it will fit in the existing load cell configuration. The PCB consists of four layers so that it was possible to connect components with vias in the PCB.

4

Simulations and results

Electromagnetic simulations were executed to verify the design that was delivered in the previous chapter. Therefore, CST Studio Suite® was used. Both the cylindrical bent interdigital capacitor and the two coupled coils were modelled and parameterized and after that simulated. This chapter will provide the results that were acquired from these simulations.

4.1. Coil simulations

The planar PCB coil was simulated. A discrete port was connected to both ends of the coil. The frequency domain solver was used to simulate the electric and magnetic fields. The scattering parameters were than calculated. Figure 4.1 shows the impedance of the coil, which was extracted from these parameters. At $f = 266$ MHz, the imaginary part becomes negative. At $f = 27$ MHz, the real part is 1.416 Ω and the imaginary part is 113.1 Ω.

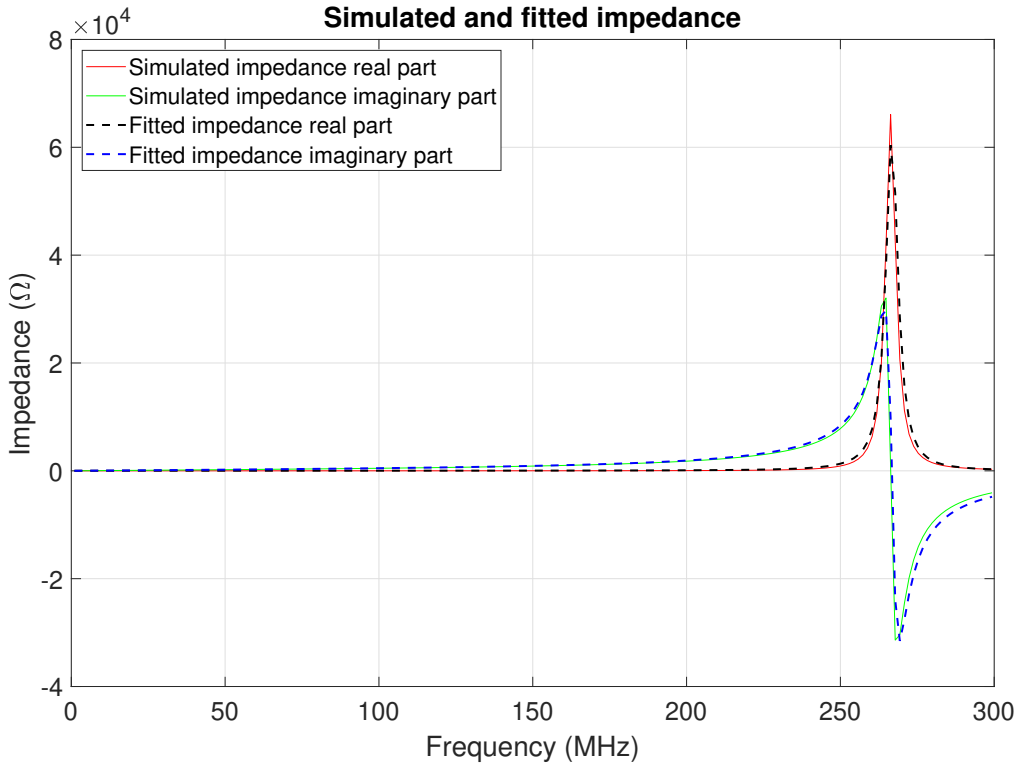

Figure 4.1: The simulated real- and imaginary part of the impedance of the planar coil.

The simulations are now fitted with the model explained in Section 3.4.2. Table 4.1 shows the values of the inductance, resistance and capacitance. The fitted impedance is also plotted in Figure 4.1. The resistance of 20 Ω is chosen to fit the peak. However, at low frequency values the simulated resistance

is much lower with R_l = 1.416 Ω. The quality factor at f = 27 MHz, calculated with Equation 3.9 is equal to Q = 79.71.

Table 4.1: Planar coil model values

Component	L_s	R_l	C_l
Value	0.66535 μH	20 Ω	0.535 pF

4.2. Capacitor simulations

The interdigital capacitor parametric model that was derived in Section 3.5.1 was modelled using CST. As mentioned in Section 3.5.3, CST is capable of simulating and deriving capacitance values. This simulation was executed for different values of n_c. CST computes the new values of the other parameters of the model and repeats the simulation and calculations. Consequently, a cylindrical bend was applied to the model, as depicted in Figure 4.2.

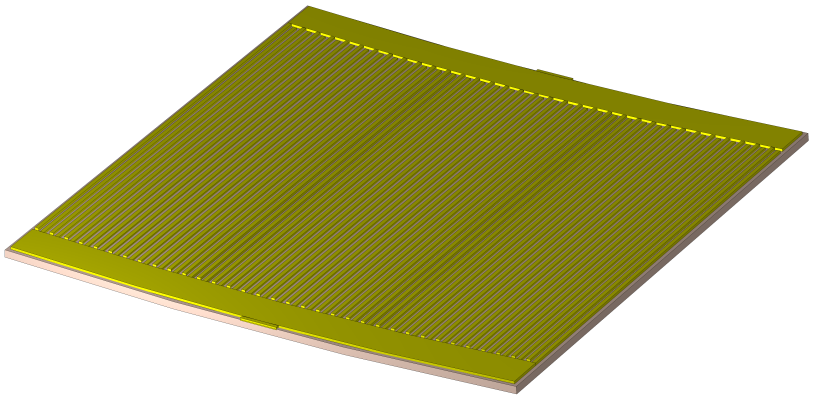

Figure 4.2: The cilindrical bent capacitor

According to Requirement SEN-MR01, this bend is limited to 0.2 mm. Therefore, the bend was adjusted to this value. Another sweep of n_c was done, and simulation and calculations were repeated using the maximally bent model. The resulting simulated capacitance values were plotted, and a curve was fitted to show the relationship between the capacitance and n_c for the non-bent and maximally bent model. The resulting plots are displayed in Figure 4.3. The fitted curves were subtracted and plotted to provide insight into the change of the capacitance (see Figure B.1 in Appendix B.1). It is concluded that the change in capacitance due to bending is limited to maximally around 0.47 pF, and may drop to around 0.4 pF when decreasing the number of fingers. However, this will also affect the absolute value of the capacitance and the resistance. Section 3.5.3 reflected on these results and gives the corresponding design choices. The capacitance change for the interdigital capacitor with 72 fingers is ΔC_s = 0.458 pF.

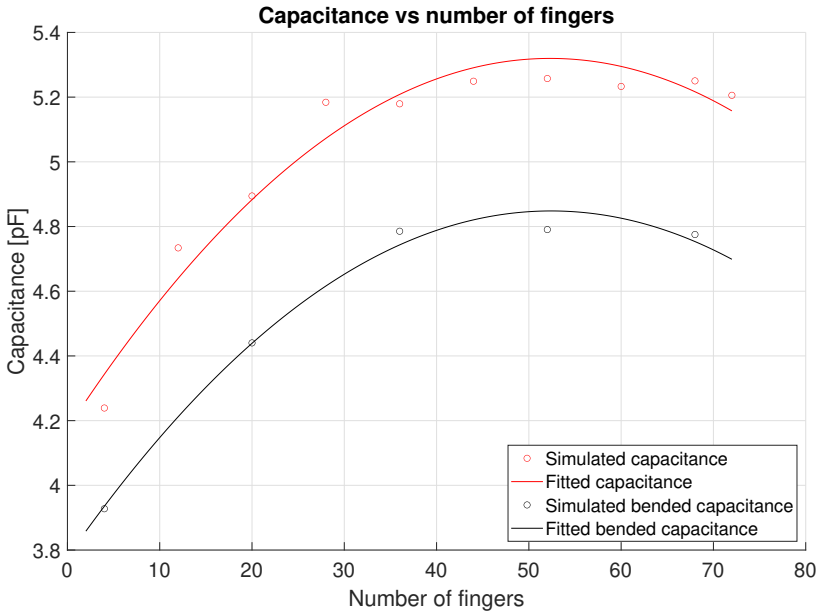

Figure 4.3: The simulated and fitted capacitance of the unbent and bent capacitor.

4.3. Coupled coil simulations

Two mirrored coils are simulated in CST. A sweep is performed for the distance between the coils from 0.5 mm to 4.5 mm. Figure 4.4 shows the simulated mutual inductance. As depicted, the mutual inductance increases and the resonance frequency decreases when the coils are brought closer together. The coupling factors that correspond to these mutual inductances at f = 27 MHz are displayed in Table 4.2.

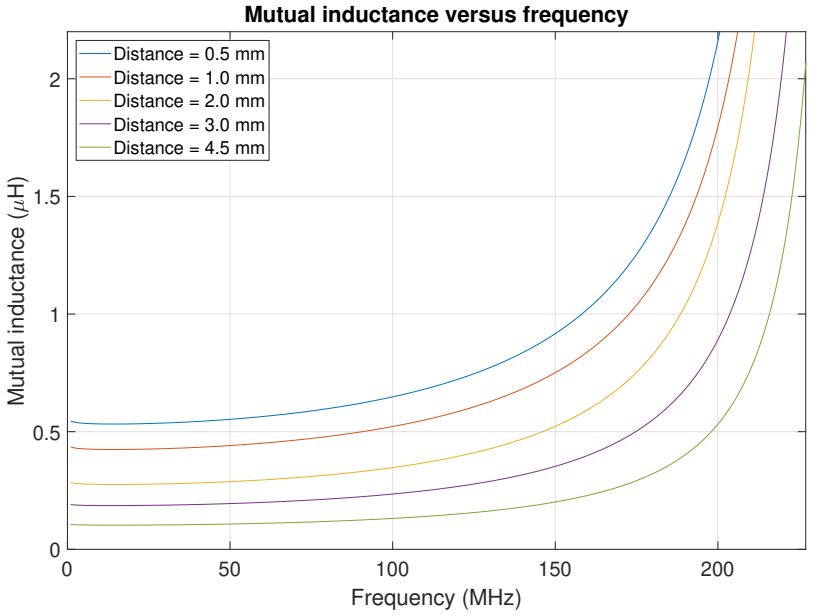

Figure 4.4: The mutual inductance of the two coupled coils at different distances.

Table 4.2: The coupling factor at different distances between the coils.

Distance	0.5 mm	1.0 mm	2.0 mm	3.0 mm	4.5 mm
k	0.80	0.64	0.42	0.28	0.16

Now the coupling process is simulated when the sensor in the belt moves across the reader coil, as depicted in Figure 4.5. One coil was horizontally displaced by 14 mm and then moved over the other coil with steps of 1 mm, until it was perfectly above the other coil. The distance between the coils was 2.0 mm.

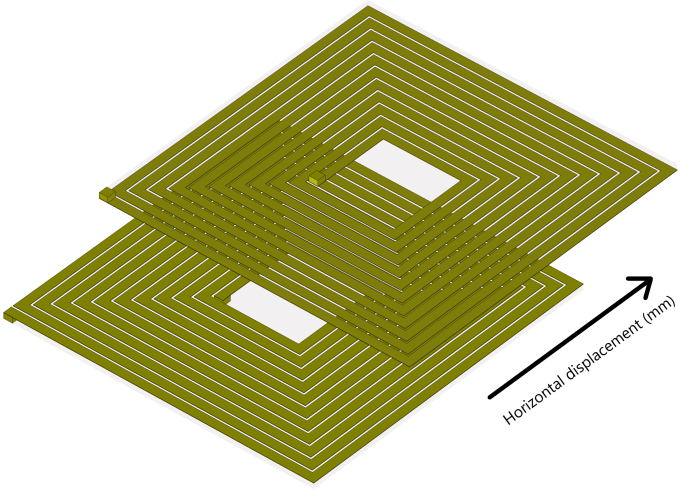

Figure 4.5: The two coils of which one is horizontally displaced.

The mutual inductance was calculated at a frequency of f = 27 MHz. From the mutual inductance, the coupling factor was calculated. The result is displayed in Figure 4.6. When the coil is displaced by 6.8 mm, the mutual inductance and coupling factor become zero.

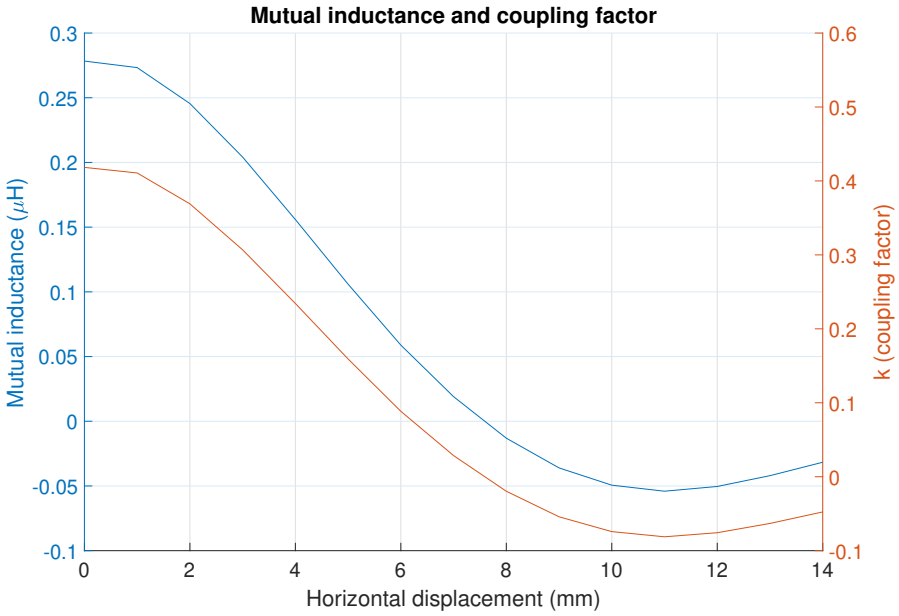

Figure 4.6: The mutual inductance and coupling factor of the horizontally displaced coils.

Finally, the worst case scenario was simulated, at a distance between the coils of 3.0 mm and the sensor coil is rotated by 10 degrees in the x-direction, 5 degrees in the y-direction and 5 degrees in the z-direction. The result is visible in Figure 4.7. k equals 0.34 in this case.

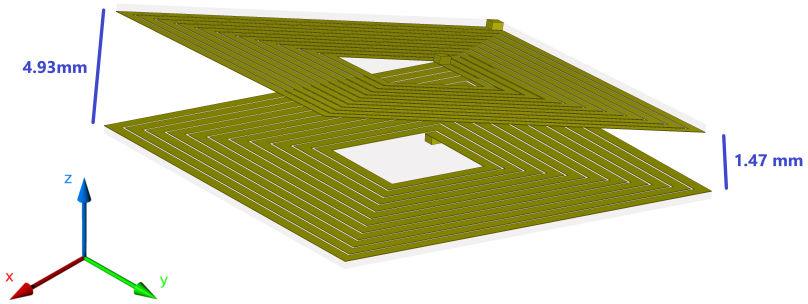

Figure 4.7: The two coils of which one is rotated.

4.4. Total sensor

The total sensor impedance, including the coupled coils, is now simulated in MATLAB (Appendix E.3). For this simulation, the circuit in Figure 3.2 and Equation 3.4 are used. Table 4.3 gives the values of the sensor from the simulations of the components. Note that R_2 is composed of resistance R_c and R_l, and that C_s is composed of C_c, C_l and C_{SMD}. For the coupling coefficient, k = 0.42 is taken. This is the value at 2.0 mm distance between the coils. Figure 4.8 shows the simulated impedance. The resonance frequency of the sensor lies at 37.8 MHz.

Table 4.3: The parameters used in the sensor circuit simulation.

Parameter	R_1	L_1	L_2	R_2	C_s	k
Value	1.416 Ω	0.66535 μH	0.66535 μH	1.465 Ω	29.735 pF	0.42

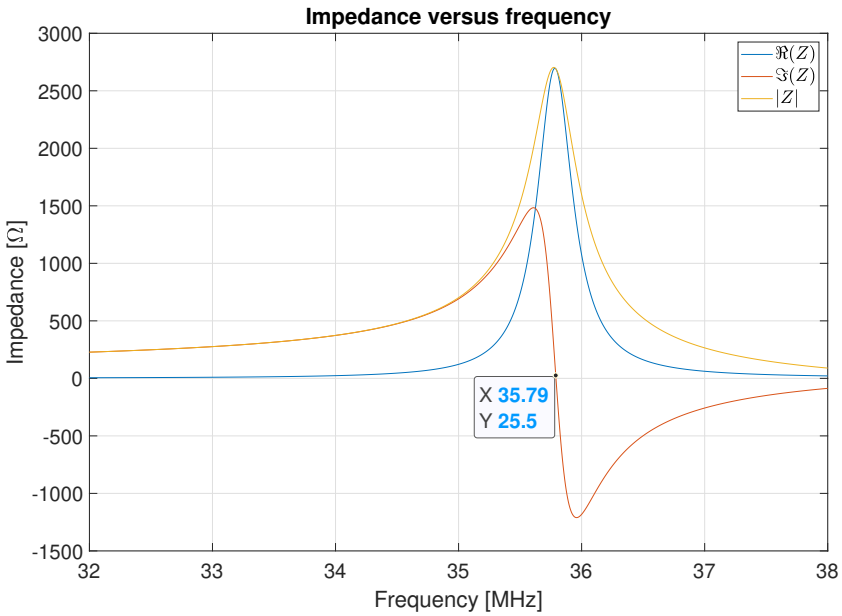

Figure 4.8: Simulated sensor impedance.

5 Discussion and verification

5.1. Discussion of results

5.1.1. Planar PCB coil

As explained in Section 4.1, the single planar PCB coil was simulated in CST and fitted with the equivalent circuit model. The inductance of the coil is 0.66535 μH. The theoretical value of the design was 1.188 μH, which is 44% higher. The resistance at f = 27 MHz is 1.416 Ω. These values yield a quality factor of Q = 79.71. The parasitic capacitance of the coil is C_l = 0.535 pF. The capacitance of the reader coil needs to be accounted for in the reader circuit because it will introduce an unwanted shift in resonance frequency. The parasitic capacitance of the sensor coil will be added to the capacitance of the interdigital capacitor. This will cause a lower sensor resonance frequency, so this capacitance also needs to be accounted for.

5.1.2. Capacitor

The resulting capacitance values from simulations were displayed in Figure 4.3. Additionally, a fitted curve is displayed, which gives an expected relationship between capacitance and n_c. The capacitances from unbent simulations were found to be at a maximum difference of 2.2% from the fitted curve. For the bent case, the difference was found to be 1.2%. The error may be further reduced by repeating the simulations several times and averaging the results or by taking smaller parameter steps. Furthermore, other forms of bending instead of cylindrical bending may lead to a larger change in capacitance value.

5.1.3. Coupling

Section 4.3 showed how the distance between the two coils affects the mutual inductance. This inductance increases when the coils are brought together, which is expected. At 0.5 mm distance, the minimal distance, the coupling factor is 0.8. At the maximum distance of 4.0 mm, the coupling factor is only around 0.20. For decreasing coupling factor, it will be more complicated for the reader to send and receive the test signal from the sensor. The resonance frequency decreases when the two coils are brought closer together. This effect is explained by Fischer and Insinger [15].

The coupling between the coils becomes zero when the coils are 6.8 mm displaced relative from each other. This is approximately half the outer diameter, d_{out} = 14.14 mm. When the sensor moves across the readout coil, it may be read out during the time it is coupled. When the belt moves with 2 m/s, the reader is coupled for 6.8 ms, see Equation 5.1. During this time, the coupling factor is greater than zero, but the effective coupling time, the time measurements may be done, is probably shorter.

$$\frac{2 \cdot 6.8 \cdot 10^{-3}\ \mathrm{m}}{2\ \mathrm{m/s}} = 6.8\ \mathrm{ms} \tag{5.1}$$

In the worst-case scenario, when the coil is maximally rotated, and the distance between the coils is 3.0 mm, the coupling factor was k = 0.34. This k is higher than the coupling factor when the coils are not rotated (k = 0.28). This difference is explained by the fact that by rotating, the coils are brought closer together at one side, while at the other side the coils are moved further apart. The coupling factor is not proportional to the distance between the coils, as may be concluded from Table 4.2. Bringing one side of the coils closer together has a more significant impact on the coupling factor than moving the other sides further apart.

5.1.4. Adjusting the value of the SMD-capacitor

As mentioned in Section 5.1.1, the value of inductance resulting from simulations equals 0.66535 μH. The inductance value that was analytically determined and used in the design, equals 1.188 μH (Section 3.4.6). Since $\omega_{res} = \frac{1}{\sqrt{LC}}$ (Equation 3.8), an decrease of L needs to be compensated with an increase in C, in order to obtain the same resonance frequency. Hence, the value of the SMD capacitor, C_{SMD}, that was suggested in Section 3.5.3, needs to be adjusted such that the resonance frequency band shifts to the right frequencies.

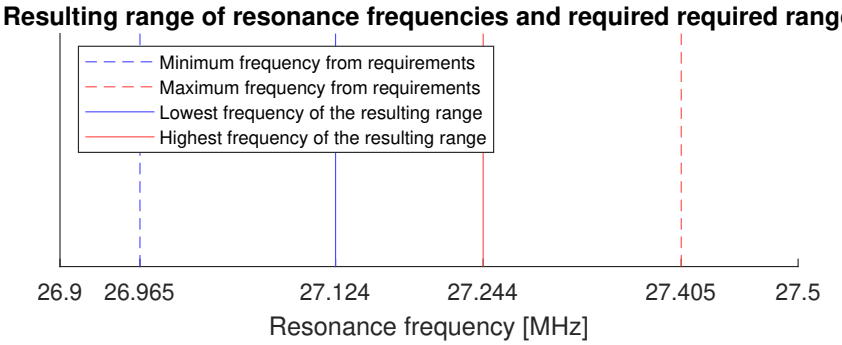

Figure 5.1: The resulting range of resonance frequencies that was found by changing C_{SMD} such that the range was set to the middle of the required frequency range

The frequency range is set to the middle of the required range (Requirement SEN-ToR03), in order to achieve most power inside this required range. This is depicted in Figure 5.1. Using Equation 3.8 multiple times results in a frequency band of 27.124 MHz to 27.244 MHz. C_{SMD} results from the subtraction of the coil capacitance and the capacitance in the bent case from the capacitance found at the lowest frequency. This subtraction gives C_{SMD}= 46.515 pF. The range of C_s values is found by subtracting the coil capacitance from the capacitance for the lowest and highest resonance frequency of the resulting frequency range. The value of C_s is found to range between 50.757 pF and 51.2135 pF. Appendix E.4 provides the corresponding MATLAB-code.

Table 5.1: Table of the resulting frequency range and capacitor values

Frequency range	C_{SMD}	C_s
27.124 MHz - 27.244 MHz	46.515 pF	50.757 pF - 51.214 pF

5.1.5. Reflection on the resulting frequency range

The range of 27.124 MHz - 27.244 MHz is relatively small compared to the frequency band from the requirements, as depicted in Figure 5.1. Only 27.5% of the entire required range is then used. This small range will make the readout of the sensor much more complex since resonance frequency will only change 120 kHz while bending from minimum to maximum. In order to increase this value, the design may be improved in several ways. First of all, the absolute value of the capacitance may be increased, by increasing the value of the SMD-capacitor. The range of resonance frequency values will then be shifted to lower frequencies. It is then required that a different frequency band is selected. It would be more desirable to increase the capacitance value of the interdigital capacitor. This solution was discussed in Section 5.1.2. Besides, the inductance may be increased. This would be at the cost of either violating, increasing the size (violating Requirement SEN-ToR01), or add an extra layer of PCB (violating Requirement SEN-ToR04). However, as depicted in Figure 3.3, increasing the inductance will not have much effect for minimal changes in capacitance. Therefore, increasing the change in capacitance value or changing the frequency range are the best options to increase the change in resonance frequency.

5.1.6. SMD-capacitor fabrication errors

Unfortunately, an SMD-capacitor may have fabrication errors, resulting in an error in the capacitance value and therefore a shift in the resonance frequency range. As long as this range still lies inside the

selected range from Requirement SEN-ToR03, this does not have to be a problem. Figure 5.2 depicts the shifts of the resulting range of the resonance frequency between the unbent case and maximally bent case, for different percentages of error in C_{SMD}. For comparison, the required range from the requirements is also displayed. As depicted in the Figure, if the error is higher than $\pm$1.3%, the range would shift out of the required band. Therefore, either a capacitor with an error lower than $\pm$1.3% should be used, or a different frequency range should be selected.

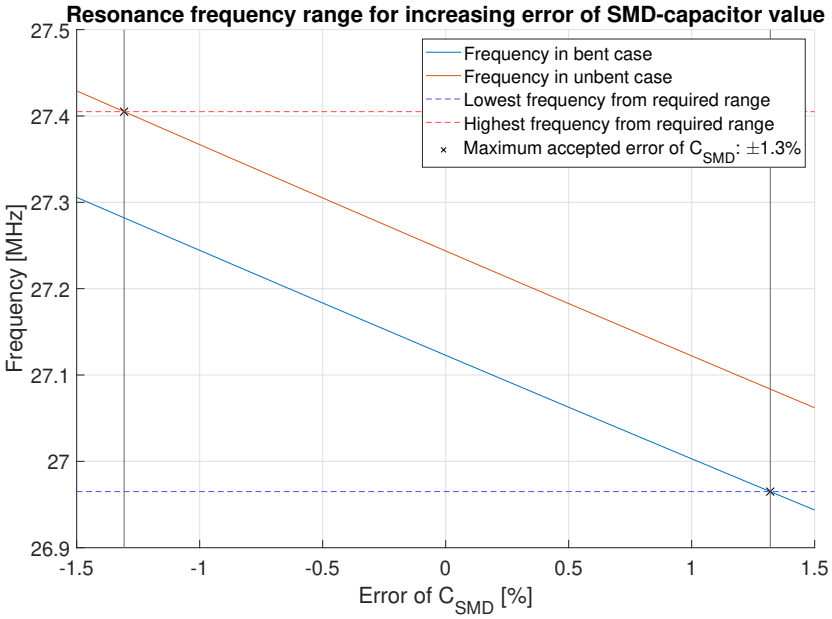

Figure 5.2: Impact of errors in the value of the SMD-capacitor on the resonance frequency range.

5.1.7. Final sensor impedance simulation

The impedance of the sensor is simulated with the new value for C_{SMD} using the MATLAB script in Appendix E.3. The figures in Appendix B.2 reveal the impedance of the unbent capacitor and the fully bent (0.2 mm) capacitor. The impedance plots show the desired behavior; the resonance frequency moves from 27.124 to 27.244 MHz while bending the interdigital capacitor.

5.2. Requirements assessment

In this section, the program of requirements will be assessed using the results. The assessment will be done for the system requirements, sensor requirements, and sensor-reader interface requirements respectively. The requirements were given in Chapter 2.

5.2.1. System requirements

Requirement SYS-MR01 specified that the sensor needed to pass information to the receiver while moving with 2 m/s. Many factors play a role in this specification, such as the power of the wireless signal from the reader circuit or the number of samples the analyser needs to obtain useful data. Due to all the different factors, it is not feasible to assess this requirement without a prototype to test it. As explained in Section 4.3, the time the coils are coupled is at most 6.8 ms. This time may be increased by increasing the quality factor or coupling.

Requirement SYS-MR02 is met because the sensor is read out using wirelessly coupled coils. Requirement SYS-ToR01 specified that the sensor readout should be invariant to temperature differences. This simulation has not been executed. With a prototype of the sensor, this requirement may be assessed. If it is variant to temperature, compensation for this may be implemented in the reader or analyser circuit.

5.2.2. Sensor requirements

Requirement SEN-MR01 is satisfied in theory. The load cell diaphragm will press on the sensor circuit and deform it. The results of the simulation of the cylindrical bent capacitor in Section 4.2 showed that the capacitance decreases with 0.47 pF. This decrease alters the resonance frequency of the sensor, which is a change in the electrical parameters of the sensor.

Requirement SEN-MR02 is satisfied in theory. In Section 4.3 simulations were performed that demonstrate that the coils are coupled for maximum horizontal displacements of 6.8 mm. The same holds for Requirement SEN-MR03. Simulations of the distance between the coils show that the coils are still coupled when they are 4.0 mm apart. Lastly, Requirement SEN-MR04 is also met in theory. A worst-case simulation was done for a distance between the coils of 3.0 mm and the maximum rotational error. The simulation shows that the rotation does not influence the coupling negatively. A prototype has to be built, and measurements have to be done in order to find out if these three requirements are satisfied. In theory, the coils are still coupled with the deviations, but as explained by Fischer and Insinger [15], the resonance frequency is also dependent on the value of k if the sensor contains a parasitic capacitance.

Requirement SEN-MR05 specified that the sensor should be passive and that preferably no batteries should be used in the sensors. This requirement is met because the sensor is designed with only passive electrical components. Requirement SEN-ToR01 specified that the size of the sensor should preferably not be larger than 2 cm in diameter. The form factor of the PCB is a square, where the load cell is circular. The sides of the PCB are $\sqrt{2} * 20$mm, which is 14.14mm. This PCB fits into the maximum dimensions, so this requirement is met. Requirement SEN-ToR02 may only be assessed when the sensor PCB is designed. The costs are as low as possible for the volume of sensors that is ordered.

As demonstrated in Section 5.1.5, the resonance frequency should, in theory, remain between the bounds that were specified in Requirement SEN-ToR03: 26.965 MHz and 27.405 MHz. In Section 5.1.4, a range of 27.124 MHz to 27.244 MHz was achieved, which lies inside this range. Furthermore, Requirement SEN-ToR04 specified that the sensor should consist of at most one piece of PCB material. This requirement is met since the sensor circuit is implemented on one PCB.

5.2.3. Reader-Sensor interface requirements

For the wireless transfer, coupled coils were used. Therefore, Requirement IF2-MR01 was met. As mentioned in Section 4.1, the parasitic capacitance of the coil was found to be equal to 0.535 pF. This value was used to assess Requirement IF2-MR02 by Fischer and Insinger [15].

Trade-off Requirement IF2-ToR01 is not met. The resistance of the PCB-coils was found to be 1.416 Ω in the simulations. This value is higher than the 0.25 Ω that was specified. This resistance is kept as low as possible, by making the traces of the PCB-coil as wide as possible. It may be considered to make the traces even wider or thicker, but this will also affect the inductance of the coil. Requirement IF2-ToR02 is met. The capacitance of the sensor is much bigger than 1 pF, due to the additional SMD-capacitor. On the other hand, Requirement IF2-ToR03 is not satisfied, since the quality factor of the coil is 79.71, according to the simulations in Section 4.1. The quality factor needs to be increased by decreasing the resistance or increasing the inductance.

Since C_s ranges between 50.757 pF and 51.214 pF, as stated in Section 5.1.4, and C_l equals 0.535 pF, Requirement IF2-ToR04 is not met. Therefore, C_s needs to be compensated by the reader circuit. This is explained by Fischer and Insinger [15]. Lastly, Requirement IF2-ToR05 was not met. The change in resonance frequency is 120 kHz, according to Section 5.1.5. This change is smaller than 0.4 MHz. In this Section, proposals were done to increase this frequency change.

6

Conclusions & recommendations

6.1. Conclusion

A passive sensor design applicable for weighing in conveyor belts was presented. It consists of a planar interdigital capacitor with an SMD-capacitor in parallel, and a square planar inductor with rectangular cross-section placed in series with the two parallel placed capacitors. The coil and capacitors form a resonance circuit, which is exited by a second coil, the readout coil, which has the same dimensions. After that, the same coupled-coils are used for the wireless readout of the resonance frequency. The components are to be placed on a PCB. This PCB is placed inside a load cell that is part of a conveyor belt. This cell will convert the weight to mechanical deformation of the PCB and the interdigital capacitor. The change in capacitance will then be read out and analyzed to calculate the weight on the cell.

A sensor type had to be selected to convert the mechanical deformation into a weight. Therefore, existing technologies designed for this purpose were examined. Based on the state-of-the-art analysis and requirements, an interdigital capacitor was selected. The design of this capacitor is possible on one PCB layer and does not need to have two plates that are placed at a fixed distance. For the wireless readout, coupled planar PCB coils were chosen, because of its simplicity, high power density, low-cost and easy fabrication. Subsequently, the resonance circuit was designed, and the ranges of values were determined based on the requirements.

Furthermore, models were developed of the coil and capacitor. Based on physical limitations, parameters of the models were fixed or expressed in terms of each other. In this way, optimal physical dimensions were calculated to ensure capacitance and inductance values in the required ranges. The values were verified using simulations.

Eventually, coil and capacitor parameters were determined. A square planar rectangular coil was chosen to fit on a square PCB made of FR-4 material. Fabrication is in-elaborate using copper traces. The coil will have 11 turns with a width of 0.40 mm, a height of 0.07 mm, an outer diameter of 14.14 mm, and an inner diameter of 3.54 mm. The turns are spaced with 0.09 mm between them, and the fill-factor will, therefore, be 0.6. In theory, this would result in an inductance of 1.188 μH, a resistance of 0.2659 Ω and a Q-factor of 757.9. In simulations, the inductance was found to be equal to 0.66535 μH and the capacitance of the coil 0.535 pF.

For the design of the sensor, a planar interdigital capacitor with 72 fingers was used. The length of a finger was chosen to be 11.85 mm, the length of the base 13.39 mm, the width of a finger 0.105 mm, the gap between the fingers 0.09 mm, and the height 0.07 mm. This design resulted in a capacitance of 5.157 pF and a resistance of 0.0485 Ω, found from simulations. This capacitor model was bent maximally at 0.02 mm, which resulted in a drop in capacitance of 0.458 pF. In order to shift the resulting resonance frequency range in the middle of the required range of 26.965MHz-27.084MHz, an extra capacitance was added in parallel to the interdigital capacitor and the sensor coil. This capacitance is found to be equal to 46.515 pF. The resulting resonance frequency range is 27.124MHz-27.244MHz.

For the readout, a reader coil with the same dimensions as the sensor coil was proposed. The coupling factor changed from 0.16-0.8 with the required distance. The coupling factor was found to drop to 0 at a horizontal displacement of 6.8 mm. The worst-case scenario of a rotational error was found to cause

the coupling factor to drop to 0.43 at 3.0 mm distance.

6.2. Future recommendations

Restrictions in sensor size and resonance frequency range have led to a capacitance change of only 0.458 pF, resulting in a shift in the resonance frequency of only 120 kHz. In order to improve this, different types of bending may be examined in order to increase the capacitance change. Furthermore, the size of the load cell may be increased to increase the capacitance value. It was suggested to add an extra capacitance such that requirements did not need to be violated. However, the value of this capacitance needs to be guaranteed to be very accurately known. If this is possible to apply on a large scale, this would be a better solution than changing the load cell dimensions. Another solution would be to use another resonating frequency range.

Furthermore, the system needs to be built and tested. It needs to be examined whether the sensor is actually able to pass over the information moving with 2 m/s and whether temperature constraints are met. Subsequently, the interaction between the load cell and the sensor should be tested. Lastly, it should be examined whether in practice a change in weight on the load cell results in a change in capacitance value as simulated.

Bibliography

[1] Orhan Akar, Tayfun Akin, and Khalil Najafi. A wireless batch sealed absolute capacitive pressure sensor. *Sensors and Actuators A: Physical*, 95(1):29–38, 2001.

[2] Aymen Ammouri, Walid Salah, Sofiane Khachroumi, Tarek Ben Salah, Ferid Kourda, and Hervé Morel. Development of a physically-based planar inductors VHDL-AMS model for integrated power converter design. *The European Physical Journal Applied Physics*, 66:20901, 05 2014. doi: 10.1051/epjap/2014130430.

[3] Kaikai Bao, Deyong Chen, Qiang Shi, Lijuan Liu, Jian Chen, Jing Li, and Junbo Wang. A readout circuit for wireless passive LC sensor and its application for GI monitoring. *Measurement Science and Technology*, May 2014.

[4] Ewald Benes, Martin Gröschl, Wolfgang Burger, and Michael Schmid. Sensors based on piezoelectric resonators. *Sensors and Actuators A: Physical*, 48(1):1–21, 1995.

[5] John C Butler, Anthony J Vigliotti, Fred W Verdi, and Shawn M Walsh. Wireless, passive, resonant-circuit, inductively coupled, inductive strain sensor. *Sensors and Actuators A: Physical*, 102(1-2): 61–66, 2002.

[6] Xuan Dai, Lili Fang, Chuanfang Zhang, and Houjun Sun. Design of a Novel Passive Wireless Integrated SAW-Based Antenna Sensor for Structural Health Monitoring. *Journal of Sensors*, 2020, 2020.

[7] Arvind Deivasigamani, Ali Daliri, Chun H. Wang, and Sabu John. 2013.

[8] Marco Demori, Marco Baù, Vittorio Ferrari, and Marco Ferrari. Interrogation Techniques and Interface Circuits for Coil-Coupled Passive Sensors, Sep 2018. URL https://www.mdpi.com/2072-666X/9/9/449/htm.

[9] Jonathan Dijkstra and Mauries van Heteren. Load cell resonance frequency analyser. Bachelor's thesis, TU Delft, Delft, The Netherlands, June 2020.

[10] Regeling gebruik van frequentieruimte zonder vergunning en zonder meldingsplicht 2015, December 2016. URL http://wetten.overheid.nl/id/BWBR0036378/2016-12-28/0.

[11] Hirohito Funato, Hiroya Kobayashi, and Tatsuaki Kitabayashi. Analysis of transfer power of capacitive power transfer system. In *2013 IEEE 10th International Conference on Power Electronics and Drive Systems (PEDS)*, pages 1015–1020. IEEE, 2013.

[12] Haksoo Choi, Sukwon Choi, and Hojung Cha. Structural Health Monitoring system based on strain gauge enabled wireless sensor nodes. In *2008 5th International Conference on Networked Sensing Systems*, pages 211–214, 2008.

[13] Natiely Hernández-Sebastián, Daniela Díaz-Alonso, Francisco Javier Renero-Carrillo, Noé Villa-Villaseñor, and Wilfrido Calleja-Arriaga. Design and simulation of an integrated wireless capacitive sensors array for measuring ventricular pressure. *Sensors*, 18(9):2781, 2018.

[14] Rui Igreja and C. Dias. Analytical evaluation of the interdigital electrodes capacitance for a multi-layered structure. *Sensors and Actuators A Physical*, pages 291–301, 05 2004. doi: 10.1016/j.sna.2004.01.040.

[15] Jasper Insinger and Rogier Fischer. Weight sensor readout system. Bachelor's thesis, TU Delft, Delft, The Netherlands, June 2020.

[16] Sang-Dong Jang and Jaehwan Kim. 2012.

[17] Mohamed Mehdi Jatlaoui, Franck Chebila, Patrick Pons, and Hervé Aubert. Working principle description of the wireless passive EM transduction pressure sensor. *The European Physical Journal-Applied Physics*, 56(1), 2011.

[18] Yi Jia, Ke Sun, Frederick Just, and Manuel Quiñones. Design and characterization of a passive wireless strain sensor. *Measurement Science and Technology*, 17:2869, 09 2006. doi: 10.1088/0957-0233/17/11/002.

[19] L. Kleczewski and S.E. Haitjema. "A passive wireless load cell for in-situ productweight and position sensing on modular plastic conveyor belts". Bachelor project proposal for Eletrical Engineering, March 2020.

[20] S. S. Mohan, M. del Mar Hershenson, S. P. Boyd, and T. H. Lee. Simple accurate expressions for planar spiral inductances. *IEEE Journal of Solid-State Circuits*, 34(10):1419–1424, 1999.

[21] M Nabipoor and Burhanuddin Yeop Majlis. 34(1):770, 2006.

[22] R. Nopper, R. Niekrawietz, and L. Reindl. Wireless Readout of Passive LC Sensors. *IEEE Transactions on Instrumentation and Measurement*, 59(9):2450–2457, 2010.

[23] S. Raju, R. Wu, M. Chan, and C. P. Yue. Modeling of Mutual Coupling Between Planar Inductors in Wireless Power Applications. *IEEE Transactions on Power Electronics*, 29(1):481–490, 2014.

[24] Michal Ulvr. Design of PCB search coils for AC magnetic flux density measurement. *AIP Advances*, 8:47505–1, 04 2018. doi: 10.1063/1.4991643.

A

PCB design

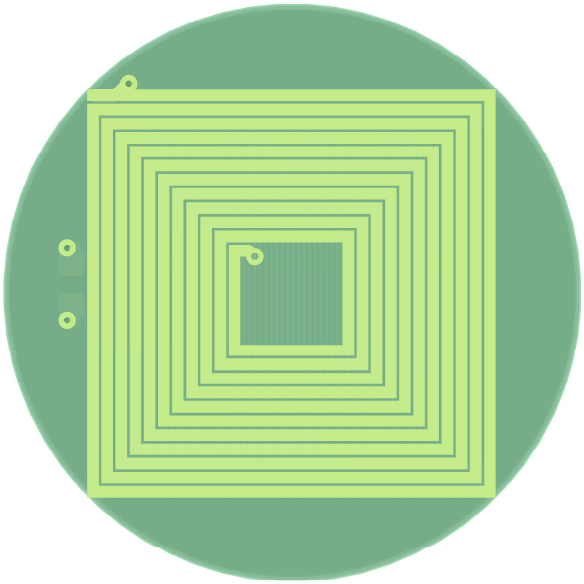

Figure A.1: Top view of the coil implemented on the PCB.

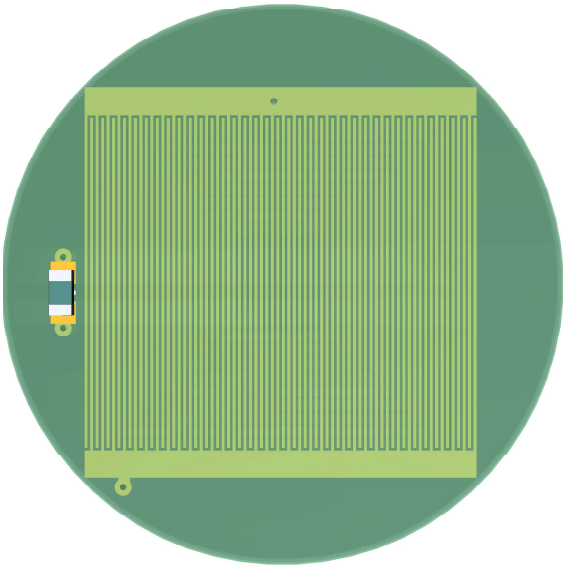

Figure A.2: Top view of the interdigital capacitor and smd capacitor on the PCB.

B

Tables and Figures

B.1. Interdigital capacitor

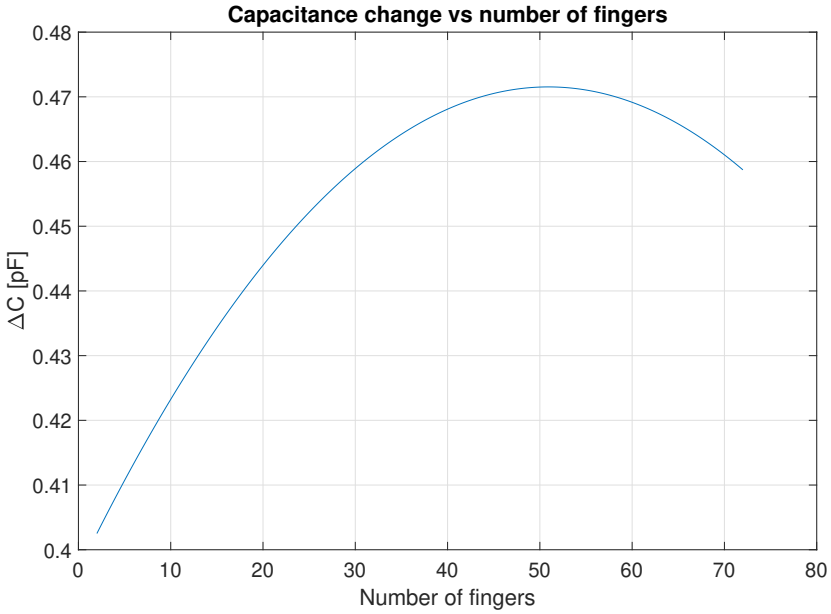

Figure B.1: The maximum change in capacitance after bending.

B.2. Final impedance simulation

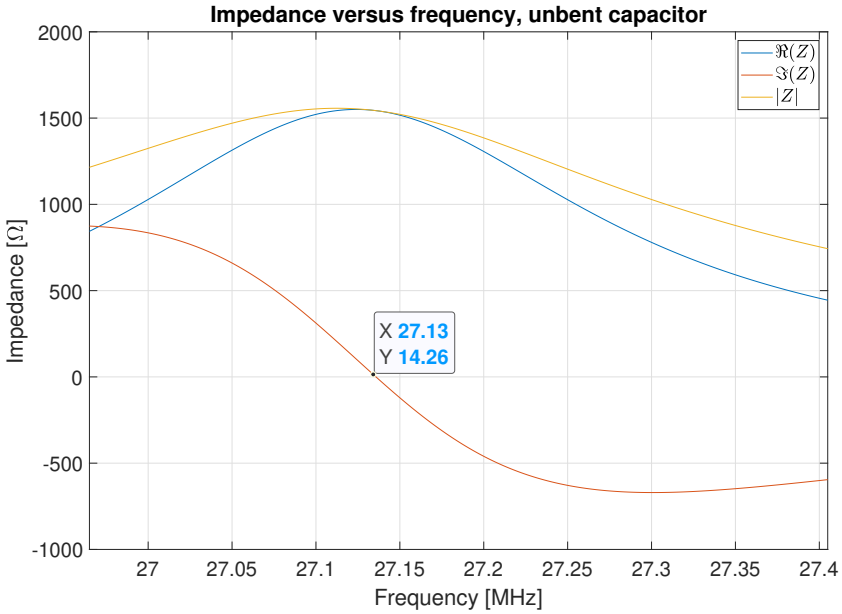

Figure B.2: Impedance of the sensor with an unbent sensor capacitor.

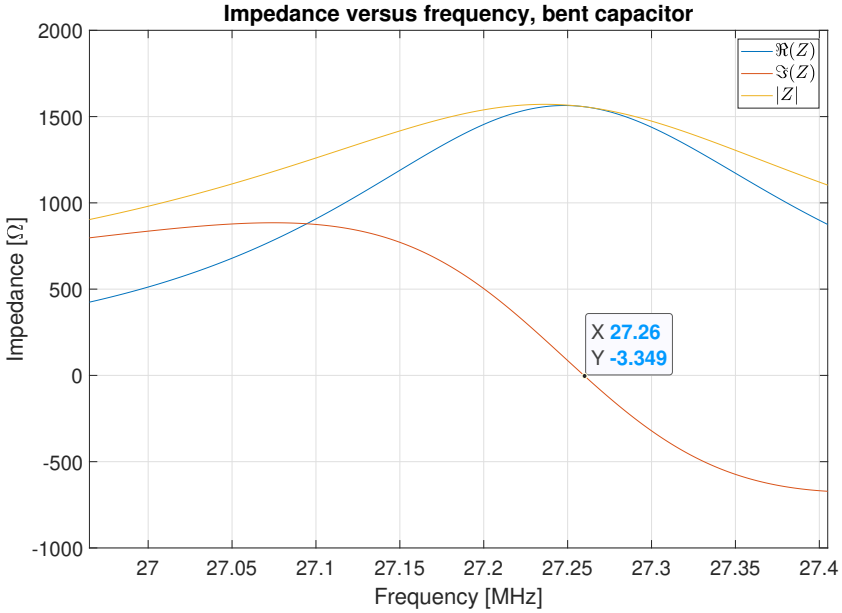

Figure B.3: Impedance of the sensor with a bent sensor capacitor.

C
Requirements

Project requirements
Analyser requirements

Table C.1: Requirements for the design of the analyser.

ID	Requirements for the design of the analyser.
FR-MR01	The analyser shall be able to detect 10 000 discrete evenly spaced levels of signal frequency.
FR-ToR01	The input signal from one sensor shall be processed within 10 ms.
FR-ToR02	The digital analyser chain shall be modeled and tested in MATLAB.
FR-ToR03	The digital analyser chain shall be implemented in VHDL and C for verification.
FR-ToR04	The analyser shall be able to communicate to a pc for further processing of the data.

Reader requirements

Table C.2: Requirements for the design of the analog reader.

ID	Requirements for the design of the analog reader.
RED-MR01	The reader shall be able to read a sensor without interference of other sensors.
RED-MR02	The reader shall be able to perform at least 10 measurements on a cell averaging the result of mechanical vibrations.
RED-MR03	The reader must generate an analog signal that enables the analyser to accurately determine the sensor change.

Interface requirements

Analyser-Reader Interface

Table C.3: Requirements for the interface between the analyser and the reader

ID	Requirements for the interface between the analyser and the reader
IF1-MR01	The voltage at the input of the analyser will be +/- 1V.
IF1-MR02	The signal frequency must be between 1kHz and 50 MHz.
IF1-MR03	The signal bandwidth must be at least 0.4 MHz.
IF1-MR04	The output impedance of FPGA is 50Ω.
IF1-MR05	The input impedance of FPGA is high.

D

Design options

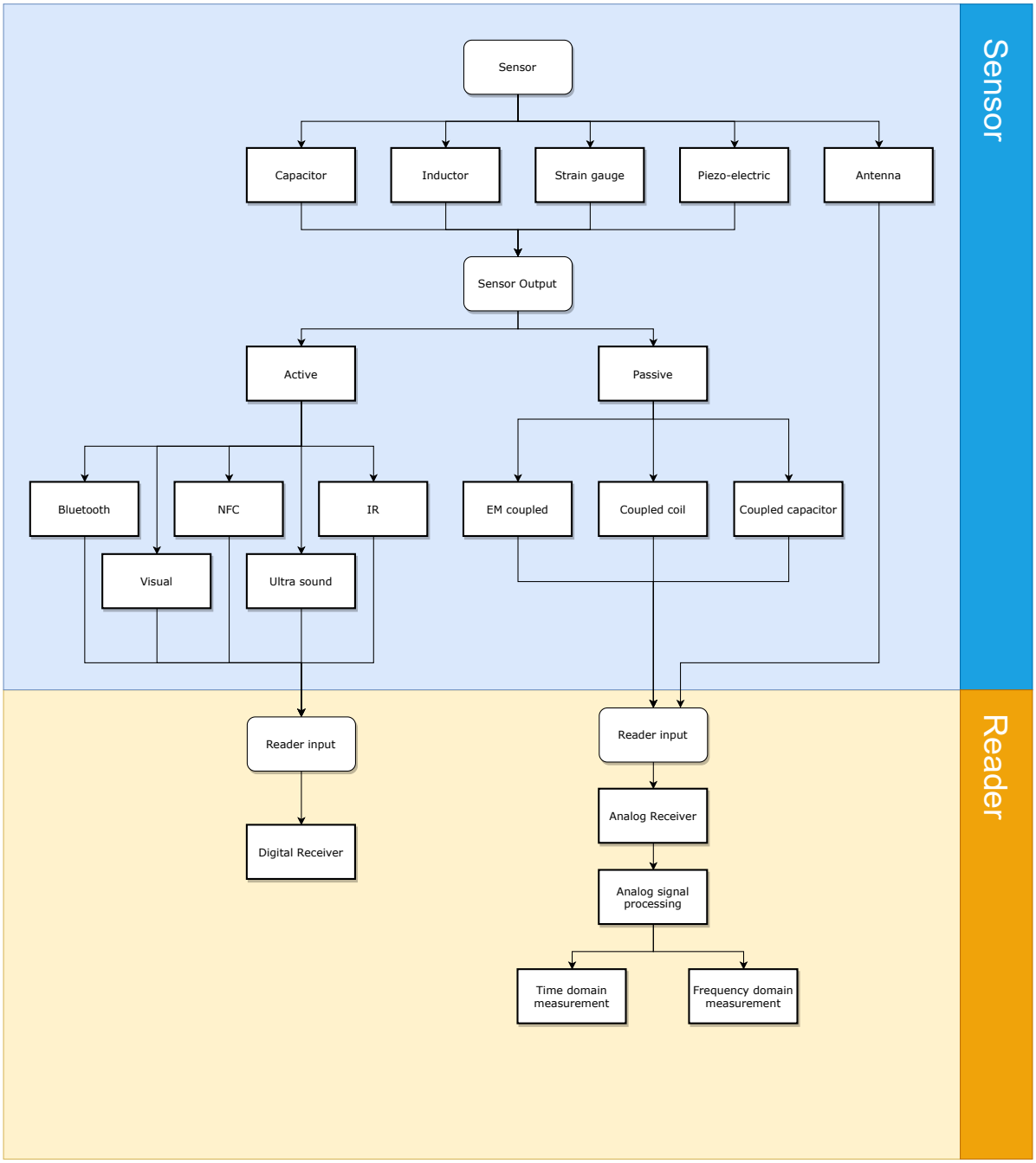

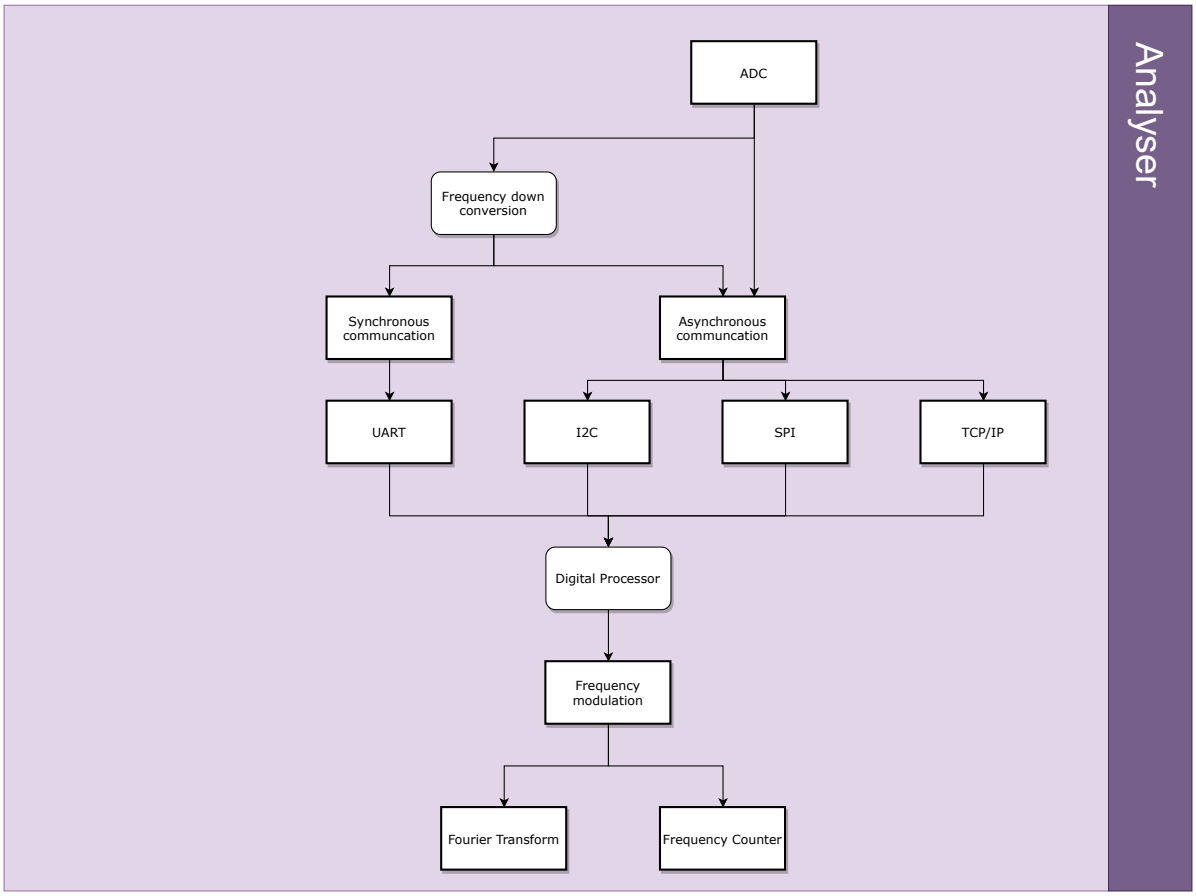
Analyser
ADC
Frequency down conversion
Synchronous communcation
Asynchronous communcation
UART
I2C
SPI
TCP/IP
Digital Processor
Frequency modulation
Fourier Transform
Frequency Counter

E

MATLAB code

Listing E.1: Matlab Script used to calculate the capacitance range and capacitance change range for different inductances.

```
%% Capacitance ranges vs Inductance
% Author: Ruben van den Bos
% Date: 16-6-2020

L=linspace(0.5e-6,6e-6,1000);

Cmin=3.37e-17./L;
Cmax=3.48e-17./L;

subplot(1,2,1)
plot(L*10^6,Cmax*10^12)
grid on
title('Capacitance vs Inductance')
xlabel('L [\muH]')
ylabel('C [pF]')
xlim([0,6])
ylim([0,65])
set(gca,'FontSize',12)
subplot(1,2,2)
plot(L*10^6,(Cmax-Cmin)*10^12)
xlim([0,6])
ylim([0,2])
xlabel('L [\muH]')
ylabel('\DeltaC [pF]')
title('Capacitance change vs Inductance')
grid on
set(gca,'FontSize',12)
```

Listing E.2: Matlab Script used to calculate the inductance of a squar or circular inductor coil.

```
%% Planar PCB coil inductance
% Author: Ruben van den Bos
% Date: 16-6-2020

clear all;

dout = 14.14; % outer diameter [mm]
gap_width = 0.09;
turn_width=0.2;
n = 20;
din=dout-2*n*turn_width-2*(n-1)*gap_width;
rho = (dout-din)/(dout+din);        % fill ratio
```

```
davg = 0.5*(dout+din)*10^-3;     % average diameter[m]
mu = 1.2566e-6;

Lmw_square = 2.34*mu*n^2*davg/(1+2.75*rho);
Lmw_circular = 2.25*mu*n^2*davg/(1+3.55*rho);
```

Listing E.3: Matlab Script used to simulate the impedance of the sensor.

```
%% Sensor impedance simulation
% Author: Rogier Fischer
% Adjusted: Ruben van den bos
% Date: 16-6-2020

L1 = 0.66535e-6;
L2 = 0.66535e-6;
Cm = 29.735e-12;
R1 = 1.416;
R2 = 1.4645;
k = 0.42;

freqs = linspace(32e6, 38e6, 1000);
omegas = freqs*2*pi;
Zs = [];

Zs = frequency_response(omegas,k,Cm,L1,L2,R1,R2);

freqs_plot = freqs/1e6;

plot(freqs_plot, real(Zs));
hold on; plot(freqs_plot, imag(Zs));
plot(freqs_plot, abs(Zs));
grid on;

xlabel('Frequency [MHz]');
ylabel('Impedance [\Omega]');
title('Impedance versus frequency')

legend('$\Re{(Z)}$', '$\Im{(Z)}$', '$|Z|$', 'Interpreter','latex')

function Z = calculate_impulse(w,k,Cm,L1,L2,R1,R2)
    Z = R1 + i*w*L1 + w^2*k^2*L1*L2*(1/(R2+i*w*L2 + 1/(i*w*Cm)));
end

function Zs = frequency_response(omega_sweep,k,Cm,L1,L2,R1,R2)
    Zs = [];
    for p = 1:length(omega_sweep)
        Zs = [Zs calculate_impulse(omega_sweep(p), k, Cm, L1, L2, R1, R2)
            ↪ ];
    end
end
```

Listing E.4: Matlab Script used to calculate the resulting resonance frequency range.

```
%% Resulting resonance frequency range
% Author: Rik Bokhorst
% Date 16-6-2020

clear all;
```

```
close all;

L = 0.66535E-6;
C_unbent = 5.157E-12;
C_bent = 4.699E-12;
C_coil = 0.535E-12;

f_min = 26.965E6;
f_max = 27.405E6;

C_min_low = 1/(L*(2*pi*f_min)^2);
C_min_high = C_min_low-(C_unbent-C_bent);
f_min_high = 1/(2*pi*sqrt(L*C_min_high));
f_high = (f_max + f_min_high)/2;
C_high = 1/(L*(2*pi*f_high)^2);
C_low = C_high+(C_unbent-C_bent);
f_low = 1/(2*pi*sqrt(L*C_low));
C_SMD = C_low - C_bent - C_coil;
C_s_high = C_high - C_coil;
C_s_low = C_low - C_coil;

xline(round(f_min*1E-6,3), 'b--');
xline(round(f_max*1E-6,3), 'r--');
xline(round(f_low*1E-6,3), 'b');
xline(round(f_high*1E-6,3), 'r');
title('Resulting range of resonance frequencies and required required
    ↪ range');
xlabel('Resonance frequency [MHz]');
set(gcf,'position',[10,10,550,200]);
set(gca,'XTick',[26.9 round(f_min*1E-6,3) round(f_low*1E-6,3) round(f_high
    ↪ *1E-6,3) round(f_max*1E-6,3) 27.5]);
set(gca,'YTick', []);
set(gcf, 'PaperUnits', 'points');
set(gcf,'PaperPosition',[0,0,900,600]);
set(gca,'FontSize',10);
lgd = legend('Minimum frequency from requirements', 'Maximum frequency
    ↪ from requirements', 'Lowest frequency of the resulting range', '
    ↪ Highest frequency of the resulting range', 'Location', 'northwest');
lgd.FontSize = 6;
```